Oman pottery as a key to the ancient Indian maritime trade: a multi-analytical approach

Daniele Zampierin, Patricia Moita, Silvia Lischi, Marike van Aerde, Pedro Barrulas, José Mirão

Abstract

The populations in Sumhuram (3rd/2nd century BC - 5th century AD) and HAS1 (1st millennium BC - 1st/2nd century AD) were involved in one of the most important examples of large-scale trade systems in the antiquity: the maritime network connecting the coasts of the Indian Ocean. Located along the Wadi Darbat in the Governorate of Dhofar, in southern Oman, both Archaeological sites are extraordinary examples of Indian maritime trade complexity. This research focuses on the chemical and mineralogical characterisation of southwestern Arabian and Indian pottery from both archaeological sites, spanning from the end of the 1st millennium BC until the 4th century AD. A multi-analytical complementary approach was carried out to characterise the ceramics and go in-depth into the provenance, as suggested by the typological attribution. The techniques used in this study were X-Ray Diffraction (XRD), ceramic petrographic, Inductively Coupled Plasma Mass Spectrometry (ICP-MS) and Scanning Electron Microscope coupled to Energy Dispersive X-ray Spectroscopy (SEM-EDS). The results obtained allowed us to identify 8 different fabric-compositional groups with very distinct geological signatures highlighting the enormous variability of raw materials origin. The groups were: Shell-Temper (ST), Shale-rich Fabric (SF), Talc-rich Fabric (TF), Basalt-rich Fabric (BF), Rice Temper (RT), Fine Fabric (FF), Medium-Large temper grains in fine Fabric (MLF) and the Shell and Sand rich Fabric (SSF). Within southwestern Arabian groups (ST, SF and TF), only ST is of Dhofar production while SF and TF originate from Yemen. Most of the typological groups defined as Indian were confirmed, but the specific typological classification does not reflect the fabric grouping. The Indian fabric-compositional groups identified underline the participation of several areas of the Indian subcontinent in the Indian Ocean trade network: Gujarat and the central-west region, south of India and the alluvial plane of the north of India. This work highlights the fundamental insights that a multi-analytical complementary approach can provide in provenance studies, especially in the compless context of the Indian Ocean trade system. The analysis also show how Sumhuram and HAS1 populations were directly and dynamically involved in the ancient Indian Ocean trade network.

Keywords: Ceramics, Oman, Indian Ocean Trade, Archaeometry, Dhofar, Inqitat, Sumhuram, Khor Rori

1. Archaeological Historical background

In Dhofar, nowadays in the Sultanate of Oman, between the end of the 3rd and the beginning of the 2nd century BC, the South Arabian kingdom of Hadramawt established a colony called Sumhuram with the probable aim of facilitating the collection of the locally produced frankincense (Buffa 2019). At that time, the Dhofar region was intensively inhabited, as highlighted by the settlement HAS1 located on the coast just a few kilometres away from Sumhuram (Lischi 2019) and the other archaeological traces found during the Trans Arabian

Expedition (Zarins 2001). Sumhuram and HAS1 are nowadays included within the same archaeological area known as Khor Rori (Figure 1).

The earliest occupation layers of the Sumhuram colony reveal the contemporary presence of southwestern Arabian[1] and Indian[2] ceramics. The coexistence of the two ceramic groups ended around the 3rd century AD, while the settlement was inhabited until the beginning of the 5th century AD (Buffa 2019). The location of the colony dominating the estuary of Wadi Darbat and the presence of warehouses along the walls towards the wadi's banks highlight the trading nature of the city (Avanzini and Pavan 2011). The archaeological site was first excavated in the 1950s by an American mission and then by IMTO[3] from the 1990s until 2019 (Buffa 2019).

HAS1 was founded within the first half of the 1st millennium BC and abandoned due to a fire by the end of 1st-beginning of 2nd century AD (Lischi 2018). The excavation of HAS1 started in 2016 under IMTO and successively continued under the DHOMIAP[4] research project. The settlement, roughly 2 hectares, was composed of more than 70 circular or sub-circular structures, and many of the artefacts retrieved were of Indian origins (Lischi 2019; Lischi *et al.* 2020).

The contemporary occupation of the two culturally diverse neighbouring settlements and the cohexistance of southwestern Arabic and Indian materials, in both sites, represent a unique context for analysing the circulation of imported and local goods within two different cultural environments. The context gives the opportunity to investicgate what type of material was reaching the Dhofar region, from where it was arriving and what type of connections there were among the local HAS1 village, the colony of Sumhuram and its motherland the Hadramawt kingdom.

2. Materials and Methods

This work presents an archaeometric approach, combined with the stylistic analyses, to the study of provenance of the southwestern Arabian and Indian ceramics found in southern Oman. Chronologically, the analysed materials (Table 1), 18 sherds from HAS1 and 17 from Sumhuram, date from the end of the 1st millennium BC to the 3rd century AD, and they express the variety of Indian and southwestern Arabian fabric and vessel types recorded within the two sites (Lischi 2019; Lischi *et al.* 2020).

[1] With "south-western Arabia" is intended the geographic area that includes nowadays Yemen that is the Dhofar region of Oman and the south-western borders of Saudi Arabia. The use of south-western Arabia as definition aims to delimit the geographical area without including any cultural or political identification.

[2] With "India" is here intended the geographical area included within the Indian Subcontinent and nowadays Sri Lanka. The use of India as definition aims to delimit the geographical area without including any cultural or political identification.

[3] Italian Mission to Oman

[4] DHOfar Map & Inqitat Archaeological Project

Within the presented study, it was used a multi-analytical approach that has already been proven extremely effective in obtaining the ceramic composition and technological characterisation (Finlay *et al*., 2012; Borowski *et al.*, 2015; Mirello *et al.*, 2015; Seetha et Velraj, 2016; Beltrame *et al.*, 2019; Tsoupra *et al.* 2022). The analytical techniques adopted[5] were thin-section petrography (optical microscopy – OM), Powder X-Ray Diffraction (PXRD), Scanning Electron Microscopy – Energy Dispersive x-rays Spectroscopy (SEM-EDS) and Inductively Coupled Plasma – Mass Spectrometry (ICP-MS). The objective was to identify the material composition and technological features of the sherds. The results are then compared with archaeological and geological data to better define the provenance of the studied ceramics.
Due to the invasive and partially destructive nature of the analysis conducted, all samples were first recorded through photography and some through 3D photogrammetry (Karasik and Smilansky, 2007; Mirulla, 2011).

2.1 Sample Preparation

To perform mineralogical and chemical analysis, a fragment of the samples (roughly 10g) was cut off using a circular Struers Discoplan saw to be less invasive. The pieces removed were then rinsed carefully with distilled water and ethanol before being dried at 40°C for 24h. The powdering was initialised by hand on an agate mortar and completed using the automatic mill Retsch PM100. The powders were then stored at 40°C to avoid moisture in the samples. Loss of ignition (LOI) was determined by the calcination of dried samples in a muffle furnace (0.5g) for 2h at 1050°C. Simultaneously, a smaller piece was cut to prepare the thin-sections. To produce 30µm thick thin-sections, the "TS method" developed by Struers was adopted with the addition of EpoDye colourant to the impregnation mix. Its adding makes it possible to measure the porosity with image processing in future studies.

2.2 Optical Microscopy (OM)

The thin-sections were analysed by means of a polarised microscope Leica DM 2500P with the camera Leica MC170 HD mounted and communicating with the Leica Application Suite V 4.4 software. The presence of minerals and rock fragments as well as matrix characteristics, porosity and sorting were described according to the scheme proposed by Quinn (2009). The sphericity and the dimensions of the grains were described using the terminology proposed by Adams *et al.* (1984).

2.3 Powder X-rays Diffraction (PXRD)

The PXRD was conducted on powdered samples using a Bruker AXS D8 Discovery XRD with the Da Vinci design, a Cu Kα source operating at 40 kV and 40 mA, and a Lynxeye 1-dimensional detector. The scans were

[5] All the sample preparation and analysis took place at the HERCULES Laboratory, University of Évora, in Évora (Portugal), except for the thin sections, which were prepared separately at the Geosciences Department of the University of Évora.

run from 3° to 75 ° 2θ, with 1 second for acquisition time and 0.05 2θ step. The PXRD allowed mineralogical bulk analysis using the ICDD[6] databases and the software Diffrac.SuiteTM provided by Bruker.

2.4 Inductively Coupled Plasma Mass Spectrometry (ICP-MS)

The ICP-MS analysis were conducted following the method used by Beltrame *et al*. (2019), which consisted of three cycles of hotplate digestion of approximately 100 mg of powdered sample in PFA Savillex® beakers. The first digestion cycle was done by adding a mixture with 2mL 47% HF (OPTIMA grade) and 0.5 mL of 65% HNO_3 (Suprapur grade) to the powdered sample and left digesting on the closed beakers for 48 h on a hotplate at ≈100 °C. After 48h, the samples were dried by evaporation. However, the evaporation was not complete to avoid the precipitation of the components and the formation of new stable compounds. Following the evaporation, the second digestion cycle with 2 mL of freshly-made Acqua Regia was initialised. The mix was left on the hotplate at 100°C for 24h. The following day, after the evaporation, the last cycle of digestion, aiming for the organic compounds, was conducted, with the addition of 2 mL of pure HNO_3 (65%) at 100°C for 24h. After drying the samples, the final solution for the trace elements was prepared by adding 1.6 mL of HNO_3 (65%) and then filled with milliQ water up to 50 mL. The aim was to reach a solution concentration of HNO_3 2%. For the analysis of the major elements, the solutions were diluted 100 fold with HNO_3 2% concentrated. The final analysis was conducted on an Agilent 8800 ICP Triple Quad (ICP-QQQ). Prior to the analysis, the equipment was calibrated with the tuning solution provided by Agilent Technologies. Moreover, a calibration curve was the selected method for quantification of the analytes, and it was prepared by the analysis of 10 differently concentrated solutions of Standard A - NHO_3 (2%) and Standard B - NHO_3 (2%) (from High Purity Standards). The concentrations reached were of 0ppb, 5ppb, 10ppb, 20ppb, 50ppb, 100ppb, 200ppb, 400ppb, 800ppb and 1600ppb. The validity of the elemental quantification of the samples was verified by the preparation of triplicates of each sample. At the same time, the accuracy of the analysis was observed by preparing and running the certified reference materials AGV-2 and W-2a simultaneously to the samples. Experimental detection limits were performed by first measuring a 0ppb solution in the acid matrix solution (HNO3 at 2%), and then a solution of 100 ppb in the same matrix of Standard A and Standard B in 11 replicates each. The quantification limits were determined as 10 times the detection limits. The results regarding major elements were then converted into oxides by stoichiometry, and their concentration normalised to 100%. The trace elements were measured in ppm and the rare earth elements (REE) results were normalised to chondrite (Sun and McDonough, 1989). A limitation of the presented technique is the impossibility of directly measuring SiO_2 concentrations. Considering the importance of having an indication of the SiO_2 quantification, the percentage of it was extrapolated by means of comparing the quantification of the major element oxides and the LOI weight data. The data was extracted by means of the difference between LOI results and the total % that the major oxides represent of the sample.

[6] International Centre for Diffraction Data

2.5 Scanning Electron Microscopy with Energy Dispersive Spectroscopy (SEM-EDS)

Micro-analysis and micro-imaging are fundamental steps toward the development of a complete dataset related to ceramic samples (Froh, 2004; Tite *et al*., 1982; Tite, 1991). The analysis was conducted with a variable pressure Hitachi S3700N SEM coupled with a Quantax EDS microanalysis system on the same thin sections previously studied by optical microscopy. The Quantax system was equipped with a Bruker Axs 5010 XFlash Silicon Drift Detector (129 eV spectral resolution at FWHM/ MnKα). The SEM-EDS quantification was done using the software ESPIRIT by Bruker. The operating conditions were the following: backscattering mode (BSEM), 20 kV accelerating voltage, 10 mm working distance, 100 μA emission current and 40 Pa pressure in the chamber. The major elements composition of the specific components within the sample matrix were converted into oxides by stoichiometry and normalised to 100%.

3. Results

3.1 Optical Microscopy (OM)

The analysis of the ceramic samples through optical microscopy (OM) highlighted the diverse nature of the samples studied, resulting in their subdivision into eight different groups. The separation was based on a combination of amount, nature, shape and dimension of temper, and technological characteristics (Table 2 and Table 3). The fabrics identified are Shell Tempered (ST), Shale-rich Fabric (SF), Talc-rich Fabric (TF), Basalt Fabric (BF), Rice Tempered (RT), Fine Fabric (FF), Medium-Large inclusion in fine Fabric (MLF) and Shell and Sand rich Fabric (SSF).

The Shell Tempered (ST) fabric is distinguishable by the significant amount (≈ 40%) of unsorted, angular shell fragments. Secondary inclusions are angular calcite and quartz grains.

The Shale-rich Fabric (SF) is mainly characterised by the presence of rounded shale clasts together with highly variable inclusions as well-preserved shells and shell fragments, calcite, micas, quartz, feldspars and amphibole with preserved euhedral forms were identified. The variability of types and dimentions of the inclusions suggests a very poor preparation of the raw material prior to ceramic production.

The Talc-rich Fabric (TF) can be divided petrographically into two subgroups. Both subgroups (TF-1 and TF-2) are characterised by the presence of talc, although with different amounts. TF-1, together with unsorted angular talc grains (≈ 10%), also includes an important amount (≈ 20%) of large shale grains and traces of calcite, quartz and opaques. On the other hand, TF-2 is composed mainly of angular talc grains (≈ 40%) of variable dimensions associated with very few quartz and chemogenic sedimentary rocks inclusions, possibly chert. The general composition of the TF-2 subgroup suggests a quite important degree of raw material preparation, with talc grains being of probable intentional addition.

The Basalt-rich Fabric (BF) is the most abundant type within the sample group. It exhibits the presence of basalt inclusions as a key characteristic. However, basalt grains are few, and their dimensions and roundness are not consistant among the samples. Despite the variability, the presence of basalt in all the samples indicates a common geographical/geological provenance. A large variability of poorly-sorted inclusions of quartz,

feldspars, opaques, pyroxene, calcite, olivine and rice husks were also identified with variations in the association of such components.

The Rice Tempered (RT) fabric group also presents traces of basalt grains. The distinction between the BF and the RT lies in the evident use of rice husks as intentionally added temper (≈ 20%) in the latter. The RT fabric is characterised by a high degree of porosity connected to the degradation of rice husks which left undisputable imprints on the material surrounding. Other authors have also noted it (Tomber *et al.*, 2011 and Lischi *et al.*, 2020). Together with rice husks and rare basalt grains, a limited amount of small quartz, calcite and opaques grains was observed by OM.

The Fine Fabric (FF) group's main characteristic is the fine material and remarkable quality of ceramic production. The few recognisable inclusions are quartz and calcite grains. The fabric is generally non-porous, and in one of the samples, there was evidence of a slip.

The Medium-Large inclusions in fine Fabric (MLF) is the second-largest group. In this group, the samples share the similar characteristic of presenting homogeneously large crystals as inclusions within a generally fine and homogenous matrix. In particular, the majority of such large inclusion grains are quartz (≈ 30%). Still, it is also possible to recognise, at subordinate amounts, the presence of feldspars, calcite, opaques phases, micas, pyroxene and detrital sedimentary rocks grains, possibly sandstones. Within this petrographic group, significant variability is mainly related to the dimension and angularity of the larger inclusions and the concentration of specific minerals.

Lastly, the Shell and Sand rich Fabric (SSF) presents some well-rounded shell fragments and well-rounded recrystallised limestone grains within a coarse sandy matrix. Within the fabric, it is also possible to recognise some quartz grains and opaques.

3.2 X-Ray Diffraction (XRD)

The global mineralogical composition was obtained by XRD on powdered samples. The results highlight the important differences between the fabric groups and the invariability within the groups, validating the previous OM observations. The summary of diffractograms interpretation is presented in Table 4.

Although the mineralogical composition shows important variations among the different fabric groups, quartz is always present and usually is one of the most abundant temper phases. Calcite represents the major mineral phase in the ST and SSF groups, agreeing with the presence of shell fragments. Calcite is abundant also within SF group sharing similar concentrations with plagioclase and amphibole.

TF group samples diffractograms reflect the high amount of talc, but a distinction can be noticed between TF-1 and TF-2 due to the higher variability in the composition of the TF-1 group. In fact, with talc, quartz and amphiboles, calcite and plagioclases are also present in this group. Otherwise, TF-2 diffractograms, beyond talc, show only some traces of quartz, calcite and micas.

In addition to the very high quartz and plagioclase concentration registered in the BF diffractograms, hematite and pyroxene are also present in significant amounts, agreeing with the basaltic nature of the temper. Furthermore, the most important characteristic recognisable is the very limited presence of calcite and the

relatively constant presence of hematite. A similar mineralogical composition is found in the diffractograms of the RT groups, underlining the similarity between the two groups as mentioned before.

MLF group diffractograms show a different mineralogy, represented by the highest quartz concentration together with K-feldspar and plagioclase.

Lastly, the FF group presents a mineralogical composition that includes quartz, plagioclase, K-feldspar and mica. Such composition is not remarkably different from other groups, especially from groups BF, MLF and RT. The distinction of the FF group from the rest of the sample was mainly textural more than compositional.

XRD analysis also allowed the recognition of phases that were impossible to identify by OM. Some of them can be important for future firing process analysis of these ceramics. In particular, the FF group is characterised by mullite in all three samples and the common presence of gehlenite separating the group from the RT samples. Furthermore, the SSF group also highlights the presence of mullite and gehlenite in every sample. The remaining fabric groups show only sporadic examples of mullite, gehlenite, spinel and wollastonite, without any evidence of consistent group-related characteristic composition.

3.3 Inductively Coupled Plasma - Mass Spectroscopy (ICP-MS):

The obtention of elementary chemical composition data aimed to validate the separation into groups made previously and possibly find chemical tracers to identify provenances. The detailed oxide values are presented in Table 5, while the trace elements results obtained with ICP-MS are presented in Table 6 and Table 7.

As presented in Figure 2, the higher variability is for Al_2O_3 and CaO that generally match with previously defined petrographic groups, allowing their individualisation as previously defined. Moreover, within each defined petrographic group, the major elemental composition exhibits a similar global elemental signature (Fig. 3).

The high CaO concentration (36,9 – 44,9 wt%) in ST samples is a distinguishing feature. This matches with the higher amount of calcite identified by PXRD and the shell fragments identified by OM. Lower enrichment in CaO (≈ 17,0 – 17,7 wt%) is presented in the SSF group that also presents high Al_2O_3 contents (10,1 – 11,6 wt%).

SF main characteristic is the relatively high Al_2O_3 concentrations (17,0-18,4 wt%), representing not only the clayish nature of the paste but also the presence of shale inclusions. Relative variability in CaO is relatable to the irregular presence of shell fragments within the different samples.

MgO is key for the distinction of the TF group, and it is directly related to the presence of talc as temper. TF-1 present a lower MgO concentration (6,6 – 8,8 wt%) and a higher CaO (7,9 – 8,8 wt%) than the TF-2. The difference can be explained by the higher compositional variability of TF-2 ceramic than TF-1, as presented before.

BF group is characterised by an Al_2O_3 concentration that ranges between 12,6 and 22,6 wt%, the highest concentration. The minor variations in Al_2O_3 and Fe_2O_3 (7,5 - 15,3 wt%) can be related to the variable-ratio inclusions/paste of the samples.

The RT samples, similarly to the BF ones, show high concentration in Al_2O_3 (12,3-13,2 wt%) and Fe_2O_3 (9,3 – 10,2 wt%). The estimation of the SiO_2 concentrations in the RT samples shows the highest values directly related to SiO_2 enrichment caused by the addition of rice husks.

Similarly to RT, also FF group, with a small number of inclusions, have high Al_2O_3, CaO and Fe_2O_3 concentrations. Chemically the main difference between RT and FF is the higher CaO concentration (7,6 – 10,4 wt%) in FF compared with RT (3,2 – 3,8 wt%).

On the other hand, MLF reaches the highest concentration of Al_2O_3 (18,6 – 26,3 wt%) of all samples. Such composition agrees with the higher feldspar amount (K-feldspar ± plagioclase) as temper.

Considering all the samples on the ternary diagram of Heimann and Maggetti (2019, Fig. 4), it is possible to notice their individualisation regarding the major elements considered. Moreover, when the stylistic distinction between Arabic and Indian material is included, a clear separation between the two provenances is identifiable with the Arabic samples characterised by an enrichment of MgO + CaO concentrations as consequence of the presence of talc and shells in the paste.

ICP-MS was also used to collect data related to trace elements, which, however, generally presented no consistent patterns to be used as tracers for fabric identification or provenance analysis. However, elements such as Ni or Cr are enriched in the TF and BF samples, which is in accordance with their more mafic composition, whereas Ba is enriched in MLF, agreeing to a greater presence of K-feldspar and biotite. Trace elements are strongly influenced by the nature of the inclusions present in the ceramic, which shows great variability within the same fabric groups.

Accordingly, with the other trace elements results, REEs also show no clear compositional trends. However, the highest REE content was found in the MLF samples, and the highest La*/Lu* ratio occurs in the same group. This indicates the presence of heavy mineral phases within MLF not detectable by XRD or OM. The trace elements and REE data are available in Tables 6 and 7.

3.4 Scanning Electron Microscopy with Energy Dispersive Spectroscopy (SEM-EDS)

Microanalysis by SEM-EDS were conducted to corroborate some textural and compositional features previously obtained by OM, to compare the chemical composition of inclusions and to complete the description of the fabrics' characteristics (Table 8).

The ST group main characteristic is the unsorted shell fragments used as temper. Their CaCO3 composition was confirmed by SEM-EDS and noticed as being occasionally associated with Si. This can result from silicification of biogenic carbonate, as mentioned by Brand (1988).

Within the SF group, it was possible to identify bone fragments confirmed by the Ca and P-rich composition. Furthermore, the elemental distribution analysis conducted on some sedimentary grains confirmed the shale nature of the grains (Al, Si, K rich) and the Mg-rich composition of amphiboles.

Observation by SEM-EDS within TF-2 confirmed the major role of the talc inclusions. However, they also highlighted the presence of evidences of biocolonization (Skadiņš et al. 2019) and the remarkable amount of iron oxide grains.

BF analysis clarified the occasional traces of rice huscks (Si-rich), the presence of basalt grains and, in some samples, of volcanic glass.

As mentioned before, RT group included a few basalt grains, confirmed by means of SEM-EDS. The presence of well-preserved rice husks was also largely confirmed by the same technique (texture and Si-rich composition). However, the elemental analysis by EDS shows that the pyroxenes found in RT paste are distinct from those analysed in the BF group, within basalt grains or in the paste (Fig. 5). This observation suggests different occurrences of basalts. On the other hand, within the same sample, the composition of the pyroxenes, as grains present within the paste of the BF sample or in basalt inclusions, is similar.

The FF group samples, when observed by SEM-EDS, highlighted some differences. One sample, namely IQM18A.US80.3, demonstrated an extremely fine matrix with hardly any inclusion. On the other hand, sample SUM10C.US162.119 resulted in very diversified microscopic inclusions, among which bone fragments were also recognisable. Furthermore, sample SUM10C.US162.119 presented a slip layer rich in Fe, opposite to the Ca-rich composition of the ceramic body.

SEM-EDS observation related to MLF confirmed the major role of quartz grains and K-Feldspar as inclusion. The elemental composition of the paste showed low CaO and important differences regarding SiO_2 and Al_2O_3. Such variations in the paste composition within the MLF groups are noticeable also in Figure 6. In the plot it is noticeable the lack of strong distinctions between the paste components of the groups with the only only remarkable distinction being identifiable between the two MLF samples plotted.

Lastly, the analysis of SSF confirmed the characteristics previously presented: shell fragments, which differ from the fragments in ST because eroded and because of their Si lacking, rounded recrystallised limestones and some rounded quartz grains.

4. Discussion:

The initial objective of the analysis was to understand how the chemically and mineralogically identified fabric groups related to the previous stylistically defined assemblages. The consequence expected was of a better understanding of the provenance of the material by means of identification of the main raw materials and/or production sites. The identification of the provenance represented the final objective of the analysis and the starting point for a better understanding of the trade connecting the Arabian Peninsula and the Indian Subcontinent.

The starting point for the provenance identification was that defined by the stylistic identification of the ceramic sherds. However, the typological identification was allowing only a distinction between material from the Indian subcontinent and material from the Arabian peninsula. The use of a multi-analytical approach

revealed that the distinction between southwest Arabian and Indian material represents only the starting point of a much more complex trade pattern.

The ratio between major elements (Al_2O_3/SiO_2 and MgO/SiO_2), crossed with previous information about Arabic and Indian origins (Fig. 7), shows that the samples tend to cluster according to the archaeometric groups and that the samples typologicaly identified as of Indian origins are clustered clearly separated from those identified as Arabic artefacts. It is, then, possible to argue that the distinction between Arabic and Indian done with the classic archaeologic stylistic approaches is insightful and correct. However, the new archaeometric approach highlighted a more complex image than the one provided by the stylistic approach, requiring geological information to get more accurate raw material provenance data.

As expectable when comparing provinces such as the Arabian and Indian peninsula, significant variability of geological features is identified. However, not all the data obtained from the analysis can be directly compared to exclusively geological formations, so, when possible, a direct comparison with archaeological materials of known origins is also presented.

The ST group stands out from all other groups for its CaO-rich (Fig. 4) composition related to the strong presence of shell fragments used as a temper. Despite the lack of a geological fingerprints, the use of shell fragments as intentionally added temper is a generally uncommon technological characteristic, but that is described as part of the ceramic tradition of the Dhofar region (Fig.11) arguing in favour of a local production of the ST fabric group (Pallecchi and Pavan, 2011; Reddy, 2015; Lischi *et al.*, 2020). The geographical location between the marine coast and the estuary makes this raw material from local shell deposits easily accessible.

The other samples included in the Arabic definition are the members of the SF and TF group. The characteristics of the SF group, as mentioned, are the contemporary presence of large shale grains, euhedral amphibole crystals and shells. The variability of temper refers to a varied geological origin (sedimentary and igneous/metamorphic for shales and amphibole, respectively), although they are probably collected in the same way as SF: within coastal or estuarine environments, given the presence of complete shells. Moreover, considering the geology of the Arabian Peninsula, associated with South Oman, only sedimentary rocks occur but, on the other hand, to the west of the peninsula (Yemen) and to the north (North of Oman), there is a greater lithological variability that could explain the association of materials so distinct in their geological origin. From figure 7, it is possible to notice how TF samples reflect the presence of talc by the higher MgO values. Talc is geologically relatable to the metamorphism of ultramafic parental rocks, which is characteristic of both the Yemenite Sarawat mountains and the Northern Oman Al Hajar mountains. Of the two possible sources of talc, the Yemenite one represents the strongest candidate when the important economic and cultural connections between Sumhuram and the South Arabian Hadramawt kingdom are considered (Pavan 2017). However, to test the possible Omani origin of the TF group, the REE patterns of the TF samples were compared (Figure 8) with those of archaeological talc stoneware published by P. Magee *et al.* (2005) from the UAE (United Arab Emirates) that share the Al Hajar mountains with Oman. The comparison between ceramic material and stoneware is not straightforward. Still, if we consider the extremely high concentration of talc in the TF-2 samples, the comparison shows a clear exclusion of the Omani talc sources from the possible origins

of the TF raw materials. Unfortunately, at the time of the publication, similar comparisons between Yemenite archaeological material and the samples studied in this paper were not possible, but it can be safely argued a Yemenite origin of the TF samples (Fig. 11). Additionally, if we consider the similar chemical composition, both global and paste composition, between SF and TF-1, the common presence of shale grains and amphiboles, in the absence of better data and archaeological material to be compared with SF, it is possible to hypothesise for a Yemenite origin of the SF group as well (Fig. 11). With such identification of the SF group provenance, the ST samples are left as the only locally produced materials of the 35 samples here analyzed.

The other fabrics represented in figure 7 are identified as Indian. However, as for the Arabic materials, also Indian materials are separated into fabric groups. The most abundant is the BF group. This group is characterised by the presence of basalt grains which is indicative of the igneous nature of the geological origins. Within the Indian subcontinent, the Deccan Trap igneous province is identifiable on the west/north-west side of the peninsula characterised by the presence of basalt layers. Direct comparison between geological or archaeological material was not possible. Still, the presence of basalt within the BF group and the fact that the Decan Trap is the major source of basalt in the Indian Subcontinent suggest a western Indian origin for the BF samples (Fig. 11).

A similar argumentation can be done in relation to the RT group, which includes rice husks as temper and small basalt inclusions. However, it was possible to compare the RT samples with archaeological material published by R. Tomber *et al.* (2011) from sites like Kuda, Dhatva, Kamrej and Baroda in the Gujarat region along the northernmost coastal exposure of Deccan Traps. The composition of the fabric (e.g. the presence of rice husks and basalts) of the published ceramics is very similar to the RT samples. Moreover, the same authors consider the unique characteristics of these homemade ceramics, using rice husks as a provenance indicator, limiting the RT origin to the coastal areas of the Gujarat region (Fig. 11).

With a different fabric and mineralogical composition, the FF samples chemically overlap some BF samples (Fig. 7). The main characteristic of the group is the very fine composition of the inclusions with a relatively high CaO concentration that can suggest a non-igneous source material. The characteristics, however, are not effective in identifying a specific geological formation. Archaeological material excavated in different sites spread in the south-eastern Indian state of Tamil Nadu included samples that display similar petrographic characteristics to those of FF. The excavated archaeological materials taken as comparison are identified as originating from North India, with the Began Bay coastal area as the most probable area (Odelli *et al.*, 2020), suggesting a possible similar source for the FF samples (Fig. 11).

The MLF group, individualised by petrographic characteristics, is also established through major elements chemical composition (Fig. 7). It is characterised by the inclusions of large crystals (mainly quartz, but also feldspars, amphiboles and calcite) with well-preserved crystal faces. These associations of angular and faced crystals can be indicative of proximal granitic parental material. Petrographic comparisons were possible with archaeological material published by E. Odelli *et al.* (2020) and identified as produced in the region of modern days Tamil Nadu. The Tamil Nadu area, however, is located within a very large igneous and metamorphic formation that includes most of the eastern side of the peninsula (Fig. 11). In order to corroborate the

relationship between the MLF group and the southern Indian ceramics, elemental composition comparisons are presented in figure 9 and 10. The data compared are from published material from Vellore archaeological site (Naseerutheen *et al.* 2014) and from archaeological data retrieved from Arikamedu, Chandraketugharh and Tamluck (Das *et al.* 2017). In both cases, the similarities between the published data and the MLF samples are evident. Another characteristic of the MLF is the great variability noticeable within the groups itself. Such limited differences can be interpreted as the result of diversified production centres within a large and geologically similar area or from the variability expected in geological materials. As a consequence, a possible conclusion would impose the need for further and much more in-detail investigation of the South Indian ceramic products to map the different production centres and their specific characteristics.

On the one hand, from a stylistic and chemical grouping point of view, SSF refers to the Indian Peninsula (Fig. 7), but the presence of shells refers, as discussed for ST, to Arabic Peninsula. In particular, the presence of very rolled shells can refer to a coastal environment with the input of quartz-feldspathic material. However, the sporadic presence of limestone (rolled) suggests a sedimentary parental geological area. Moreover, the limited concentration of shell fragments and their size being similar to that of other inclusions possibly exclude the intentionality of the shell addition. Due to the very common coastal clay nature of the raw material used for the the production of SSF and the lack of comparable materials and data, it is not possible to define the provenance of the SSF group from an archaeometric point of view.

5. Conclusions

The multi-analytical approach was demonstrated to be determinant for the material characterisation of the ceramics and of the provenance of most of the samples. From an initial Arabic vs Indian typological division, the adopted multi-analytical approach highlighted the more complex classification of the archaeological material and, by extension, allows to get a more detailed idea of the trade system network crossing the Indian Ocean.

The enormous variability of materials found within the site is reflected in the results obtained from several techniques confirming the very dynamic nature of the trade system that involved Sumhuram and HAS1. Eight groups were identified. The integration of all data and comparison with available archaeological information allowed the refinement of the provenances. Three groups were identified as from the Arabic peninsula: ST as local material, SF and TF as from Yemen. Despite the non-local nature of the SF and TF samples, they should not be considere as foreign materials since they are the product of the same South Arabian culture of the founders of Sumhuram. SF an TF could, then, be considered as “culturally local”.

Two groups (i.e. BF and RT) have their origin in NW India as indicated by the presence of basalts and rise husks, characteristics of ceramics from Gandara and neighbouring regions. The participation of southern and northeast Indian continent regions in the Indian Ocean trade routes is underlined by the presence of the FF and MLF ceramics. Lastly, for the SSF group, no clear provenance could be established.

This work reveals the necessity of expanding the knowledge of the ceramic fabrics involved in the trade to then be able to narrow down the provenance area even more with the creation of a clearer map of production and distribution of the traded goods.

This work has spread light over the complex cultural and economic exchange within which the settlements of HAS1 and Sumhuram were involved between the 3rd century BC and the 5th century AD. The analysis presented above demonstrated that, within the two settlements, it was possible to identify materials from diverse regions concluding the research with more of a complex image than what it was understood before. As a consequence new and more diversified questions related to the complexity of the Indian Ocean trade network developed from this work than actual answers. Furthermore, the presented paper highlights the potentiality and the importance of a multi-analythical approach towards the study of the Indian Ocean trade system. In doing so, the paper ought to sustain and demonstrate the need for a new wave of multy-analythical studies focused on the materials found acccross the Indian Oean in order to expand the understanding of Indian Ocean trade system.

6. Bibliography:

- Avanzini, A., Pavan, A., 2011. Sumhuram, a South Arabian port, in: Avanzini, A. (Ed), Along the aroma and spice routes. The harbour of Sumhuram, its territory and the trade between the Mediterranean, Arabia and India. Bandecchi e Vivaldi, Pontedera (Pisa), pp. 43-56.
- Adams, E.A., Mackenzie, W.S., Guilford, C., 1984. Atlas of Sedimentary Rock Under the Microscopes. Longman Group, Harlow.
- Brand, U. 1988. Morphochemical and replacement diagenesis of carbonates. In: Chilingarian, K. H. (Ed.), Diagenesis IV, Developments in Sedimentology 51. Wolf Elsevier, pp. 529.
- Beltrame, M., Liberato, M., Mirão, J., Santos, H., Barrulas, P., Branco, F., Gonçalves, L., Candeias, A., Schiavon, N., 2019. Islamic and post Islamic eramics from the town of Santarém (Portugal): The continuity of ceramic technology in a transforming society. J. Archaeol. Sci.: Reports 23, 910–28. https://doi.org/10.1016/j.jasrep.2018.11.029.
- Borowski, M. P., Furmanek, M., Czarniaka, K., Guia, P., 2015. Steatite-tempered pottery of the Stroke Ornamented Ware culture from Silesia (SW Poland): a Neolithic innovation in ceramic technology. J. Archaeol. Sci. 57, 207-222.
- Buffa, V., 2019. Sumhuram The Becoming of the Town Khor Rori Report 4. L'Erma di Bretschneider, Roma.
- Das, S.K., Ghosh, S., Gangopadhyay, K., Ghosh, S., Hazra, M., 2017. Provenance Study of Ancient Potteries from West Bengal and Tamil Nadu: Application of Major Element Oxides and Trace Element Geochemistry. Man and Environ. XLII (2): 11–20.
- Eggins, S.M., Woodhead, J.D., Kinsley, L.P.J., Mortimer, G.E., Sylvester, P.J., McCulloch, M.T., Hergt, J.M., Handler, M.R., 1997. n! Zi-internal standardisation. Chem. Geol. 1, 311–326. https://doi.org/10.1016/S0009-2541(96)00100-3.
- Finlay, A.J., McComish, J.M., Ottley, C.J., Bates, C.R., Selby, D., 2012. Trace element fingerprinting of ceramic building material from Carpow and York Roman fortresses manufactured by the VI Legion. J. Archaeol. Sci. 39, 2385–2391. https://doi.org/10.1016/j.jas.2012.03.002.
- Froh, J., 2004. Archaeological ceramics studies by scanning electron microscopy. Hyperfine Interact. 154, 159–176.

- Heimann, R.B., M., Maggetti, 2019. The struglle between thermodynamics and kinetics: Phase evolution of ancient and historical ceramics. EMU Notes in Mineralogy 20, 6, 233-281. https://www.researchgate.net/publication/337905856.
- Hettiarachchi, P., Motha, J. T.S., Pitawala, H. M.T.G.A., 2010. Identification of an Appropriate Body Composition for Red Clay Products (Identificação de Uma Composição Adequada Para Produtos de Argila Vermelha). Ceramica 56, 285–90.
- Karasik, A., Smilansky, U., 2008. 3D scanning technology as a standard archaeological tool for pottery analysis: practice and theory. J. Archaeol. Sci. 35, 1148-1168. https://doi.org/10.1016/j.jas.2007.08.008.
- Lischi, Silvia 2018. Inqitat Archaeological Mission Inqitat Archaeological Mission Fourth and Fifth Season of the Italian Mission to Oman (IMTO) in Season of the Italian Mission to Oman (IMTO) in the Site of Inqitat - Khor Rori Archaeological Site, Dhofar, Sultanate of Oman 28.
- Lischi, Silvia 2019. Inqitat Archaeological Mission Nqitat Archaeological Mission Sixth and Seven Season's of the Archaeological Mission Archaeological Mission in the Site of Inqitat - Khor Rori Archaeological Site, Dhofar, Sultanate of Khor Rori Archaeological Site, Dhofar.
- Lischi, S., Pavan, A., Fusaro, A. 2020. Preliminary Investigations on the 116 Local Pottery in Dhofar (Southern Oman) from the Iron Age to the Islamic Period. IASA News Res. Ctry. (25), 15–17.
- Magee, P., Barber, D., Sobur, M., Jasim, S., 2005. Sourcing Iron Age softstone artefacts in southeastern Arabia: results from a programme of analysis using inductively coupled Plasma-Mass Spectrometry/Optical Emission Spectrometry (ICPMS/OES). Arab. Archaeol. Epigr. 16, 129–143.
- Mirulla, F., 2011. LA FOTOGRAFIA ARCHEOLOGICA DIGITALE - Dallo Scatto All'elaborazione. Edipuglia srl., Bari.
- Miriello, D., Bloise, A., De Luca, R., Apollaro, C., Crisci, G.M., Medaglia, S., Taliano Grasso, A., 2015. First compositional evidences on the local production of Dressel 2–4 amphorae in Calabria (Southern Italy): characterisation and mixing simulations. Appl. Phys. Mater. Sci. Process. 119, 1595–1608. https://doi.org/10.1007/s00339-015-9143-y.
- Naseerutheen, A., Chandrasekaran, A., Rajalakshmi, A., Ravisankar, R., 2014. Elemental Analysis of Ancient Potteries of Vellore Dist, Tamil Nadu, India by ED-XRF Technique with Statistical Approach. Beni-Suef University J. Basic Appl. Sci. 3: 45– 51. http://dx.doi.org/10.1016/j.bjbas.2014.02.006.
- Odelli, E., Selvaraj, T., Perumal, J., Palleschi, V., Legnaioli, S., Raneri, S., 2020. Pottery Production and Trades in Tamil Nadu Region: New Insights from Alagankulam and Keeladi Excavation Sites. Herit. Sci. 8: 1–13. https://doi.org/10.1186/s40494-020-00402-2.
- Ottley, C.J., Pearson, D.G., Irvine, G.J., 2003. A routine method for the dissolution of geological samples for the analysis of REE and trace elements via ICP-MS. In: Grenville, H.D., Tunner, S. (Eds.), The Proceedings of the 5th International Conference on Plasma Source Mass Spectrometry Held at the University of Durham on 8–13 September 2002. The Royal Society of Chemistry, Cambridge, pp. 221–230. https://doi.org/10.1039/9781847551689-00221.
- Pallecchi, P., Pavan, A., 2011. Local raw materials used by craftsmen and in the development of the city of Sumhuram in: Avanzini, A. (Ed.), Along the aroma and spice routes. The harbour of Sumhuram, its territory and the trade between the Mediterranean, Arabia and India. Bandecchi e Vivaldi, Pontedera (Pisa), pp. 81-95.
- Pavan, A., 2017. A Cosmopolitan City on the Arabian Coast: The Imported and Local Pottery from Khor Rori. Khor Rori Report 3. L'Erma di Bretschneider, Roma.
- Quinn, P. S., 2009. INTERPRETING SILENT ARTEFACTS Petrographic Approaches to Archaeological Ceramics. Archaeopress, Oxford.
- Reddy, A., 2015. Sourcing Indian Ceramics in Arabia: Actual Imports and Local Imitations. Proc. Semin. Arab. Stud. 45, 253–272.

- Rougeulle, A., 2008. A medieval trade entrepôt at Khor Rori? The study of the Islamic ceramic from Hamr al-Sharqiya, in: Avanzini, A. (Ed.), A Port in Arabia between Rome and the Indian Ocean, 3rd C. BC - 5th C. AD: Khor Rori report 2. L'Erma di Bretschneider, Roma. http://digital.casalini.it/2640190.
- Seetha, D., Velraj, G., 2016. Characterisation and Chemometric Analysis of Ancient Pot Shards Trenched from Arpakkam, Tamil Nadu, India. J. Appl. Res. Technol. 14: 345–53. http://dx.doi.org/10.1016/j.jart.2016.08.002.
- Skadiņš, I., Micko, L., Zvaigzne, L., Narkevica, I., Kroiča, J., 2019. Adhesion and Colonisation of Microorganisms on Porous TiO_2 and TiO_2-Silver Biomaterials. Proc. Latvian Acad. Sci., Section B, 73: 325–31.
- Sun, S. S., McDonough, W. F., 1989. Chemical and isotopic systematics of oceanic basalts: implications for mantle composition and processes. Geol. Soc. Special Publication 42: 313–45.
- Tite, M.S., Freestone, I.C., Meeks, N.D., Bimson, M., 1982. The use of scanning electron microscopy in the technological examination of ancient ceramic. In: Olin, J., Franklin, A. (Eds.), Archaeological Ceramics. Smithsonian Institution Press, Washington, DC, pp. 256.
- Tite, M. S. 1991. The impact of electron microscopy on ceramic studies. Br. Acad. 77: 111–131. https://www.thebritishacademy.ac.uk/sites/default/files/77p111.pdf.
- Tomber, R., Cartwright, C., Gupta, S., 2011. Rice Temper: Technological Solutions and Source Identification in the Indian Ocean. J. Archaeol. Sci. 38: 360–366.
- Tsoupra, A., Clist, B., da Conceição Lopes, M., Moita, P., Barrulas,. P., da Piedade de Jesus, M., da Silva Domingos, S., Bostoen, K. and Mirão, J., 2022. A multi-analytical characterization of fourteenth to eighteenth century pottery from the Kongo kingdom, Central Africa. Sci Rep, Sci. Sci Rep 12, 9943. https://www.nature.com/articles/s41598-022-14089-x
- Zarins, J., 2001. The Land of Incense: Archaeological Work in the Governorate of Dhofar, Sultanate of Oman, 1990-1995: the project of the National Committee for the supervision of archaeological survey in the Sultanate Ministry of Information. Sultan Qaboos University Publications, Oman.

TABLES:

Table 1: List of the samples analysed in this paper and of relative information available before the archaeometric approach.

Sample code:	*Site*	*Excavation Year*	*Layer*	*Vessel Type*	*Fabric Type**	*Proposed Provenance*
SUMW03A.US1.1	SUM	2003	1	Bowl	Steatite Temper Ware	Local
SUM08B.US162.104	SUM	2008	162	Bowl	Steatite Temper Ware	Local
SUM11A.US174.232	SUM	2011	174	Lid-cum-Bowl	Coarse Red Ware	Indian
SUM09A.US297.2	SUM	2009	292	Carinated or globular pot	Grit Temper Ware	Indian
SUM10C.US162.119	SUM	2010	162	Bowl	Red Slipped Ware	Indian
SUM11A.US54.85	SUM	2011	54	unidentified shape	Fine Red Slipped Ware	Indian
SUM08A.US253.5	SUM	2008	253	Carinated or globular pot.	Coarse Red Ware	Indian
SUM10C.US174.79	SUM	2010	174	Bowl	Coarse Red Ware	Indian
SUM03A.US133.9	SUM	2003	133	Carinated or globular pot	Coarse Red Ware	Indian
SUM10A.US405.3	SUM	2010	405	Carinated or globular pot	Coarse Red Ware	Indian
SUM10C.US174.104	SUM	2010	174	Shallow Bowl	Vegetable Temper Ware	Indian
SUM10A.US412.1	SUM	2010	412	Carinated or globular pot	Vegetable Temper Ware	Indian
SUM10C.US174.83	SUM	2010	174	Lids-cum-Bowls	Coarse Red Ware	Indian
SUM03B.US93.23	SUM	2003	93	Table Jar	Coarse Red Ware	Indian
SUM09B.US309.4	SUM	2009	309	Lamp/lid	Coarse Red Ware	Indian
SUM03B.US93.42	SUM	2003	93	unidentified shape	Coarse Red Ware	Indian
SUM08B.US975.4	SUM	2008	975	unidentified shape	unidentified fabric type	Indian
IQM16B.US35.8	HAS1	2016	35	Pot	Shell Temper Ware	Local
IQM18B.US119.5	HAS1	2018	119	Table/storage use	Shell Temper Ware	Local
IQM17A.US58.5	HAS1	2017	58	Jar	Shell Temper Ware	Local
IQM17A.US58.8	HAS1	2017	58	Jar	Steatite Temper Ware (?)	Local
IQM16B.US35.34	HAS1	2016	35	Jar	Steatite Temper Ware (?)	Local (?)
IQM16B.US35.35	HAS1	2016	35	unidentified shape	Steatite Temper Ware (?)	Local

IQM16B.US35.33	HAS1	2016	35	unidentified shape	Steatite Temper Ware	Local
IQM16B.US35.32	HAS1	2016	35	unidentified shape	Steatite Temper Ware	Local
IQM16B.US30.6	HAS1	2016	30	Jar	Coarse Red Ware (?)	Indian
IQM16B.US30.3	HAS1	2016	30	Jar	Coarse Red Ware	Indian
IQM17A.US35.16	HAS1	2017	35	Jar	Coarse Red Ware	Indian
IQM16B.US35.31	HAS1	2016	35	Red Ware	Coarse Red Ware	Local
IQM17A.US35.18	HAS1	2017	35	Pot	Coarse Red Ware	Indian
IQM16B.US30.10	HAS1	2016	30	Jar (?)	Coarse Red Ware (?)	Indian
IQM18A.US80.3	HAS1	2018	80	Jar	Black Slipped Ware	Indian
IQM16B.US35.9	HAS1	2016	35	Jar	Coarse Red Ware	Indian
IQM17B.US73.1	HAS1	2017	73	Storage use (?)	Red Slipped Ware (?)	Indian
IQM16B.US23.13	HAS1	2016	23	Paddle Ware	Paddle Impressed Ware	Indian

*According with A. Pavan (2017)

Table 2: Schematic presentation of the identified fabric groups, of their main characteristics according to OM.

Group	Samples	Main characteristic
Shell Tempered **(ST)**	• IQM16B.US35.8 • IQM17A.US58.5 • IQM18B.US119.5	• Angular shell fragments used as temper • Quartz and carbonates inclusions
Shale-rich Fabric (SF)	• IQM17A.US58.8 • IQM16B.US35.34 • IQM16B.US35.35	• Rich in medium-large and rounded shale grains • Identification of shell fragments, calcite crystals, micas, quartz, feldspars and amphiboles as inclusions
Talc-rich Fabric (TF)	• IQM16B.US35.33 (TF-1) • IQM16B.US35.32 (TF-1) • SUMW03A.US1.1 (TF-2) • SUM08B.US162.104 (TF-2)	• Talc crystals • TF-2 with unsorted talc crystals as temper • Large variety in inclusions within TF-1 • Shale grains identified in TF-1
Basalt-rich Fabric (BF)	• IQM16B.US30.6 • IQM117A.US35.16 • IQM16B.US30.3 • IQM17A.US35.18 • IQM16B.US35.31 • SUM11A.US174.232 • SUM09A.US297.2 • SUM08B.US975.4 • SUM11A.US54.85	• Variable concertation and dimensions of Basalt grains • Plagioclases, quartz and pyroxenes as major inclusions • Micas, hematite, anatase (commonly identifiable). • Presence of rice husks and volcanic glass in some samples
Rice Tempered (RT)	• SUM10C.US174.83 • SUM10A.US412.1 • SUM10C.US174.104	• Rice husks used as temper • Presence of small rounded basalt grains • Small to extremely small and rounded quartz, crystalline calcite and opaques as inclusions
Fine Fabric (FF)	• SUM10C.US162.119 • IQM16B.US30.10 • IQM18A.US80.3	• Very fine matrix composition with limited inclusions • Inclusions of various types: quartz, plagioclase and micas • IQM18A.US80.3 presents an extremely fine matrix • SUM10C.US1662.119 with bone fragments and Fe-rich slip different from the Ca-rich core
Medium-Large inclusions in fine Fabric (MLF)	• SUM10A.US405.3 • SUM03A.US133.9 • IQM16B.US35.9 • IQM17B.US73.1 • IQM16B.US23.13 • SUM08A.US253.2 • SUM10C.US174.79	• Medium-Large temper grains (between 100µm and 500µm) • Majority of inclusion composed by Quartz and Feldspars • The grog is generally fine and homogeneous
Shell and Sand rich Fabric (SSF)	• SUM03B.US93.23 • SUM03B.US93.42 • SUM09B.US309.4	• Rich in well-rounded shell fragments • Quartz grains and recrystallised limestones as other major inclusions • Common presence of feldspars and micas.

Table 3: XPL images presenting the composition of each sample analysed. The pictures have a 0,2mm scale.

IQM16B.US35.8 (ST)

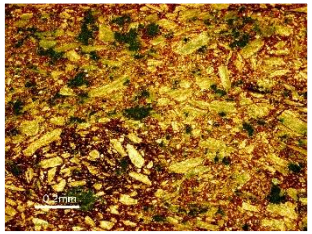

IQM17A.US58.5 (ST)

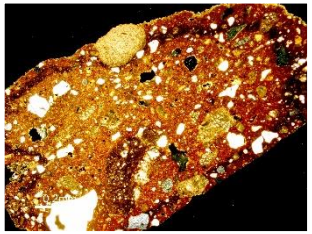

IQM18B.US119.5 (ST)

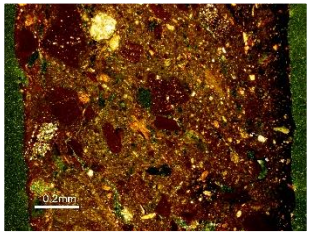

IQM17A.US58.8 (SF)

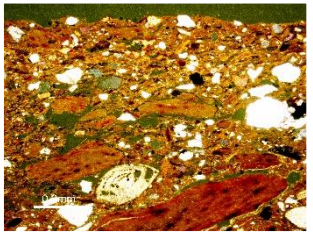

IQM16B.US35.34 (SF)

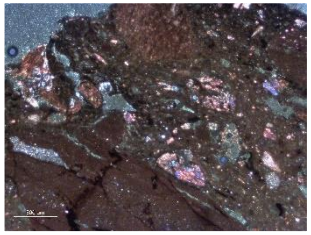

IQM16B.US35.35 (SF)*

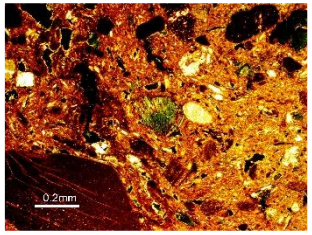

IQM16B.US35.33 (TF-1)

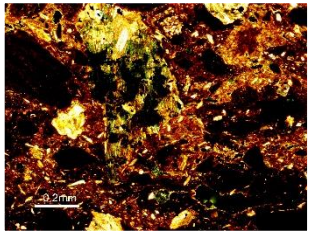

IQM16B.US35.32 (TF-1)

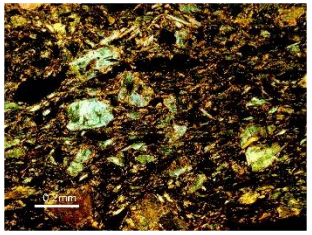

SUMW03A.US1.1 (TF-2)

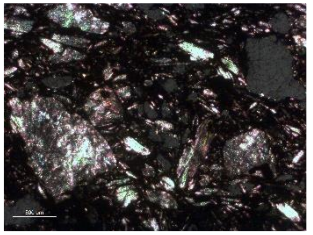

SUM08B.US162.104 (TF-2) *

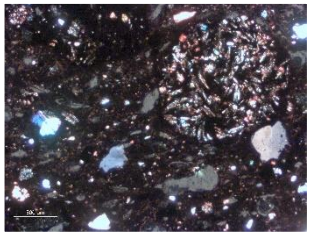

IQM16B.US30.6 (BF)*

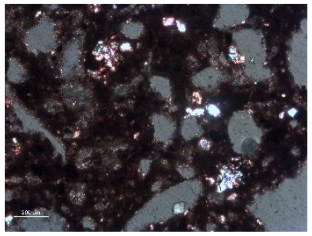

IQM17A.US35.16 (BF)*

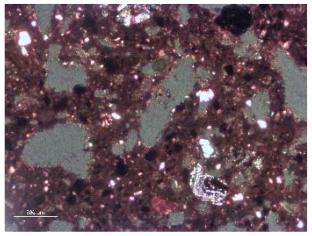

IQM16B.US30.3 (BF)*

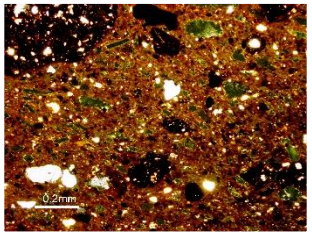

IQM17A.US35.18 (BF)

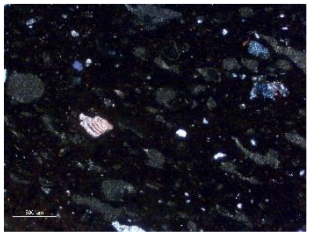

IQM16B.US35.31 (BF)*

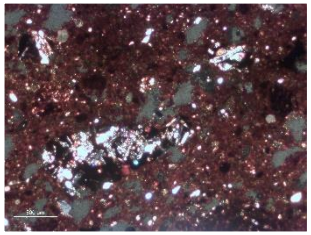

SUM11A.US174.232 (BF)*

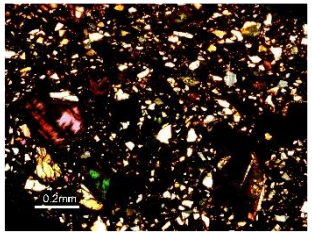

SUM09A.US297.2 (BF)*

(*) pictures with scale 500 µm
ST: Shell Tempered; SF: Shale-rich Fabric; TF: Talc-rich Fabric; BF: Basalt-rich Fabric; RT: Rice Tempered; FF: Fine Fabric; MLF: Medium-Large inclusions in fine Fabric; SSF: Shell and Sand rich Fabric.

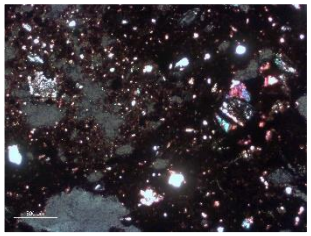

SUM08B.US975.4 (BF)*

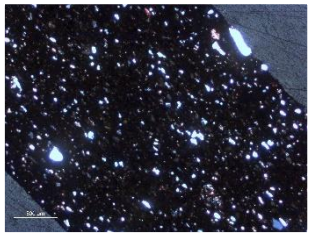

SUM11A.US54.85(BF)*

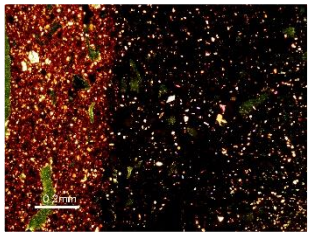

SUM10C.US174.83 (RT)

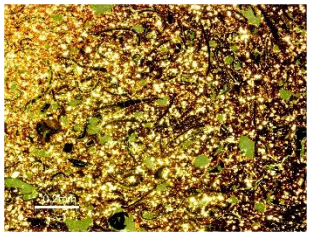

SUM10A.US412.1 (RT)

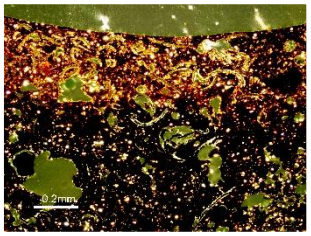

SUM10C.US174.104 (RT)

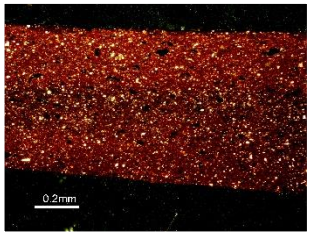

SUM10C.US162.119 (FF)

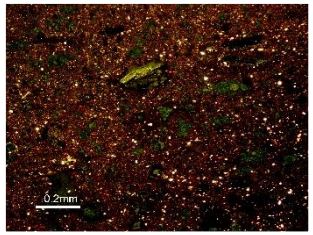

IQM16B.US30.10 (FF)

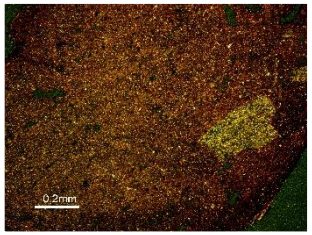

IQM18A.US80.3 (FF)*

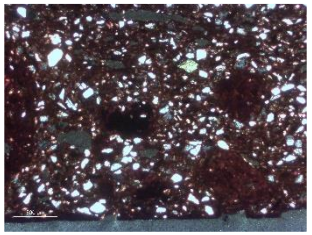

SUM10A.US405.3 (MLF)*

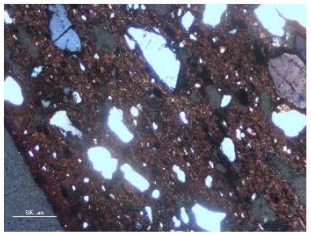

SUM03A.US133.9 (MLF)*

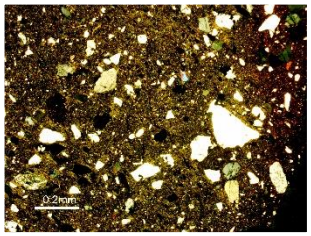

IQM16B.US35.9 (MLF)

IQM17B.US73.1 (MLF)

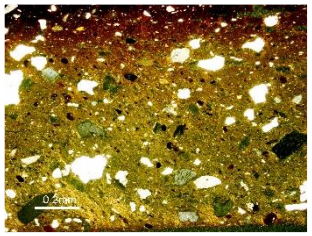

IQM16B.US23.13 (MLF)

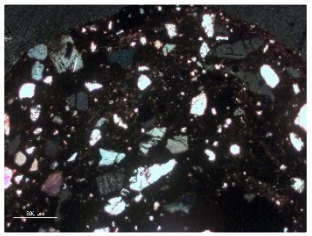

SUM08A.US253.5 (MLF)*

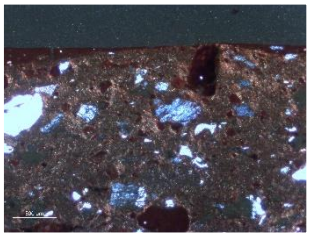

SUM10C.US174.79 (MLF)*

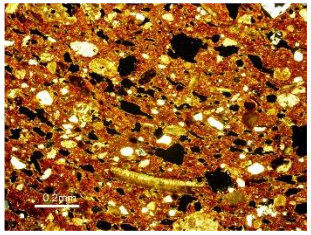

SUM03B.US93.23 (SSF)

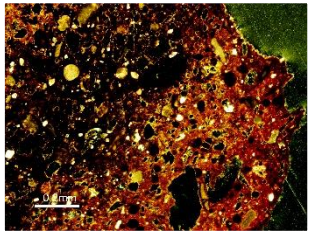

SUM03B.US93.42 (SSF)

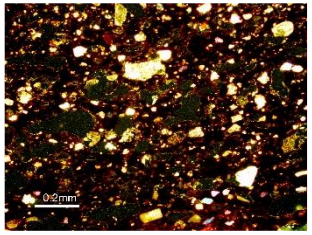

SUM09B.US309.4 (SSF)

(*) pictures with scale 500 µm
ST: Shell Tempered; SF: Shale-rich Fabric; TF: Talc-rich Fabric; BF: Basalt-rich Fabric; RT: Rice Tempered; FF: Fine Fabric; MLF: Medium-Large inclusions in fine Fabric; SSF: Shell and Sand rich Fabric.

*Table 4: XRD results for each sample grouped in the following order: ST, SF, TF, BF, RT, FF, MLF and SSF. The phases connected to the firing temperature of the ceramic are separated from the other phases and highlighted by *.*

	Sample Name	Q	C	Do	Pl	K-F	H	M	Ol	Py	Am	An	Ta	Gy	Ze	Ch	Ka	Go	Si	Rh	Sp*	Cr*	Di*	Mu*	Ge*	Wo*
ST	IQM16B.US35.8	x	xxxx	-	-	-	-	xx	-	-	-	-	-	-	-	-	-	-	-	-	-	-	x	-	-	-
	IQM17A.US58.5	xx	xxxx	-	-	-	-	x	-	-	-	-	-	-	-	-	-	-	-	-	-	-	x	-	-	-
	IQM18B.US119.5	xxx	xxx	-	-	-	-	x	-	-	-	-	-	-	-	-	-	-	-	-	-	-	x	+	-	-
SF	IQM17A.US58.8	xx	xxx	-	x	-	-	x	-	-	xx	-	-	-	-	xx	-	-	-	-	-	+	-	x	-	-
	IQM16B.US35.34	xx	x	-	xx	-	-	xx	-	-	xx	-	-	-	-	-	-	-	-	-	-	-	x	-	-	-
	IQM16B.US35.35	xx	x	-	xx	-	x	-	-	-	xxx	-	-	-	-	-	-	-	-	-	-	-	x	-	x	-
	IQM16B.US35.33	xx	x	-	x	-	-	-	-	-	xx	-	xxx	-	-	xx	-	-	-	-	-	-	x	-	-	-
TF	IQM16B.US35.32	x	x	-	x	-	-	-	-	-	xx	-	xxx	-	x	-	x	-	-	-	-	-	+	-	-	-
	SUMW03A.US1.1	x	+	-	-	-	-	x	-	-	-	-	xxxx	-	+	x	-	-	-	-	-	-	-	-	-	-
	SUM08B.US162.104	+	+	-	-	-	+	+	-	-	-	-	xxxx	+	-	+	-	-	-	-	-	-	-	-	-	-
	IQM16B.US35.31	xx	x	x	xxx	-	+	x	-	-	-	x	-	-	-	-	-	-	-	-	-	-	x	-	-	-
BF	IQM16B.US30.6	xx	-	x	xx	-	x	-	-	-	x	x	-	x	-	-	-	-	-	-	-	-	x	-	-	-
	IQM17A.US35.16	xxx	x	-	xx	-	x	-	-	-	-	x	-	-	-	-	-	-	-	-	-	-	x	x	-	-
	IQM16B.US30.3	xx	-	x	xx	-	x	xx	-	x	-	x	-	xx	-	-	-	-	-	-	-	-	x	-	-	-
	IQM17A.US35.18	xx	x	-	xxx	-	x	-	-	xx	-	x	-	-	-	-	-	-	-	-	-	-	-	-	-	-
	SUM11A.US174.232	xxx	x	-	xx	-	x	xx	-	-	-	+	-	-	-	-	-	-	-	-	-	-	x	-	-	-
	SUM09A.US297.2	xx	x	-	xxx	-	x	x	-	x	-	-	-	+	-	-	-	-	-	x	-	+	-	-	-	-
	SUM08B.US975.4	xx	+	-	xx	x	x	xx	x	-	-	-	-	-	-	-	-	-	-	-	x	-	x	-	+	-
	SUM11A.US54.85	xxx	x	-	xx	-	x	x	-	x	-	-	-	-	-	-	-	-	-	-	-	+	x	-	-	-
RT	SUM10A.US412.1	xxx	+	-	xx	-	-	x	-	x	-	-	-	-	-	-	-	-	-	-	-	-	-	-	-	x
	SUM10C.US174.104	xxx	+	-	xx	xx	-	xx	x	x	-	-	-	-	-	-	-	-	-	-	-	-	-	-	-	-
	SUM10C.US174.83	xxx	+	-	xx	x	x	x	-	-	-	-	-	-	-	-	-	-	-	-	-	-	x	x	-	-
FF	IQM16B.US30.10	xxx	x	-	xx	-	+	xx	-	-	-	-	-	xx	-	-	-	-	-	-	-	-	x	x	+	-
	SUM10C.US162.119	xxx	x	-	xx	xx	+	xx	-	-	-	-	-	-	-	-	-	-	-	-	-	+	x	x	x	-
	IQM18A.US80.3	xxx	x	-	x	x	+	xx	-	-	-	-	-	-	-	-	-	-	-	-	-	-	x	x	-	-
	SUM10A.US405.3	xx	-	-	xx	xx	-	x	-	-	xx	-	-	-	-	-	-	-	-	-	-	-	-	-	-	-
MLF	IQM16B.US35.9	xxx	-	x	x	xx	-	xx	-	-	-	+	-	-	-	-	-	x	x	-	-	-	x	-	-	x

	IQM17B.US73.1	xxxx	+	-	x	xx	-	-	-	-	-	x	-	-	-	-	-	x	-	-	-	-	-	x	-	-
	IQM16B.US23.13	xxx	+	-	xx	xx	-	-	-	x	-	-	-	-	-	-	-	-	-	-	-	-	x	-	-	-
	SUM08A.US253.5	xx	+	-	xx	xx	-	x	-	-	x	-	-	-	-	-	-	-	-	-	-	-	-	-	-	-
	SUM10C.US174.79	xxx	-	-	x	xx	-	xx	-	x	-	-	-	-	-	-	-	-	-	-	-	-	-	x	-	-
	SUM03A.US133.9	xxx	-	-	-	xx	+	x	-	-	-	-	-	-	-	-	-	-	-	-	-	-	-	x	-	-
SSF	SUM03B.US93.23	xxx	xx	-	x	x	-	xx	-	-	-	-	-	-	-	-	-	-	-	-	-	-	-	x	+	x
	SUM09B.US309.4	xx	xxx	-	x	x	+	x	-	x	-	-	-	+	-	-	-	-	-	-	-	-	x	x	x	-
	SUM03B.US93.42	xx	xx	-	x	x	-	xx	-	-	-	-	-	-	-	-	-	-	-	-	-	-	x	x	x	-

xxxx = between 70% and 100 %; **xxx** = between 40% and 70%; **xx** = between 10% and 40%; **x** = less than 10%; **+** = present; **-** = absent

Q= Quartz; **C**= Calcite; **Do**= Dolomite; **Pl**= Plagioclase; **K-F**= K-feldspars; **H**= Hematite; **M**= Micas; **Ol**= Olivine; **Py**= Pyroxene; **Am**= Amphiboles; **Ta**= Talc; **Gy**= Gypsum; **Ze**= Zeolite; **Ch**= Chlorite; **Ka**= Kaolinite; **Go**= Goethite; **Si**= Sillimanite; **Rh**= Rhodonite; **Sp**= Spinel; **Cr**= Cristobalite; **Di**= Diopside; **Mu**= Mullite; **Ge**= Gehlenite; **Wo**= Wollastonite; **(*)** = related to ceramic firing temperature

Table 5: Major elemental composition (wt. %) per sample. SiO2 is highlighted in yellow because of its indirectly measured values.

Groups	Sample Name	Na_2O	MgO	Al_2O_3	P_2O_5	K_2O	CaO	TiO_2	MnO	Fe_2O_3	SiO_2
ST	IQM16B.US35.8	0,30	2,12	6,83	0,04	1,20	36,93	0,37	0,07	3,99	48,16
	IQM17A.US58.5	0,30	1,62	4,88	0,17	1,09	44,96	0,23	0,03	2,85	43,88
	IQM18B.US119.5	0,27	2,31	4,24	0,08	0,48	38,74	0,37	0,06	2,89	50,56
SF	IQM17A.US58.8	1,14	4,14	17,43	0,12	2,34	12,06	0,97	0,05	5,93	55,82
	IQM16B.US35.34	2,05	5,33	18,45	1,08	2,93	9,04	1,27	0,07	7,67	52,10
	IQM16B.US35.35	1,58	5,11	17,06	0,14	2,30	15,81	0,89	0,08	7,31	49,72
TF-1	IQM16B.US35.33	1,74	6,61	13,69	0,19	2,80	7,96	0,93	0,07	7,54	58,47
	IQM16B.US35.32	1,88	8,89	12,30	0,28	2,47	8,83	0,83	0,09	8,45	55,99
TF-2	SUMW03A.US1.1	1,00	24,59	8,13	0,10	1,87	1,83	0,44	0,07	6,98	54,99
	SUM08B.US162.104	0,69	17,16	11,35	0,16	1,64	2,17	0,67	0,08	9,03	57,05
BF	IQM16B.US35.31	1,45	2,60	22,60	0,38	1,23	5,09	3,84	0,10	7,79	54,93
	IQM16B.US30.6	1,86	2,71	21,62	0,34	1,37	4,14	3,20	0,11	7,71	56,94
	IQM17A.US35.16	1,43	2,54	22,49	0,36	1,16	5,00	3,75	0,09	7,49	55,69
	IQM16B.US30.3	2,00	3,07	18,11	0,42	1,45	6,33	2,99	0,10	7,59	57,96
	IQM17A.US35.18	1,62	3,36	19,08	0,32	1,38	4,58	3,30	0,10	8,30	57,96
	SUM11A.US174.232	1,78	3,61	12,64	0,70	2,37	4,05	2,61	0,27	12,99	58,99
	SUM09A.US297.2	1,80	2,75	19,50	0,12	0,50	5,98	2,01	0,17	12,62	54,55
	SUM08B.US975.4	1,93	2,92	13,81	0,34	2,02	3,69	3,25	0,21	15,26	56,56
	SUM11A.US54.85	1,86	4,29	14,59	0,26	1,99	5,45	1,63	0,13	10,21	59,58
RT	SUM10A.US412.1	1,80	2,21	13,24	0,48	2,19	3,21	1,88	0,13	10,21	64,64
	SUM10C.US174.104	2,01	2,21	12,34	0,43	2,69	3,72	1,88	0,15	9,86	64,71
	SUM10C.US174.83	1,54	2,46	12,28	0,64	2,43	3,84	1,90	0,13	9,26	65,52
FF	IQM16B.US30.10	1,51	3,90	14,30	0,42	2,88	10,45	1,09	0,15	8,57	56,74
	SUM10C.US162.119	1,19	3,51	14,66	0,31	2,95	7,68	1,05	0,10	7,51	61,04
	IQM18A.US80.3	2,25	4,76	14,76	0,18	2,98	8,74	0,84	0,12	6,69	58,69
	SUM10A.US405.3	2,57	1,73	19,21	0,23	3,37	2,25	1,10	0,06	8,58	60,90
	IQM16B.US35.9	0,94	0,80	25,44	0,09	1,99	1,81	1,25	0,02	4,60	63,06
	IQM17B.US73.1	0,49	0,62	26,31	0,09	1,12	1,07	2,36	0,03	3,50	64,41

MLF	IQM16B.US23.13	1,09	0,96	24,15	0,14	2,61	1,71	1,11	0,02	4,30	63,91
	SUM08A.US253.5	2,76	1,24	18,59	0,16	3,53	2,29	1,04	0,02	8,04	62,32
	SUM10C.US174.79	1,59	0,63	22,28	0,42	3,08	1,91	1,38	0,02	6,54	62,17
	SUM03A.US133.9	1,32	0,78	21,13	0,33	2,17	1,25	1,98	0,02	9,10	61,94
SSF	SUM03B.US93.23	1,03	1,92	10,92	0,31	2,26	17,32	0,78	0,08	5,65	59,74
	SUM09B.US309.4	1,01	2,30	10,13	0,67	2,50	17,73	0,66	0,10	5,60	59,31
	SUM03B.US93.42	1,02	2,29	11,60	0,25	2,80	17,02	0,64	0,05	6,01	58,31

Table 6: Trace elements composition per sample (ppm).

Sample Name	Sc	V	Cr	Co	Ni	Cu	Zn	Ga	Ge	Rb	Sr	Y	Zr	Nb	Cd	Sn	Sb	Cs	Ba
IQM16B.US35.8	6,93	102,16	117,61	17,77	77,74	18,96	32,07	8,03	1,33	76,56	389,49	10,99	41,98	5,79	0,23	1,36	0,36	4,65	273,11
IQM17A.US58.5	6,93	74,29	81,70	9,73	48,54	13,02	29,05	6,03	1,12	44,12	428,56	9,73	33,28	4,26	0,48	0,84	0,23	2,17	91,63
IQM18B.US119.5	5,28	45,32	43,41	5,09	20,31	6,83	34,68	6,77	1,35	17,66	588,02	10,84	43,26	6,26	0,42	0,84	0,21	0,88	128,62
IQM17A.US58.8	14,62	101,73	95,84	19,38	55,57	13,76	45,95	16,95	2,18	47,73	369,59	16,76	83,38	10,45	0,71	1,69	0,22	3,08	248,18
IQM16B.US35.34	19,89	150,11	140,63	21,72	62,27	29,12	78,64	20,57	2,87	75,97	546,40	16,51	80,25	11,62	0,43	2,75	0,23	4,36	321,68
IQM16B.US35.35	14,84	96,96	93,65	25,76	72,42	31,41	66,13	18,53	2,55	57,93	287,84	24,92	118,38	10,82	0,39	2,12	0,26	2,65	306,61
IQM16B.US35.33	15,73	130,96	121,92	31,67	135,77	22,12	76,94	19,38	3,16	53,85	199,88	23,63	135,57	11,27	0,36	2,12	0,25	2,27	356,29
IQM16B.US35.32	14,13	101,90	333,03	44,94	228,10	22,28	88,56	20,14	3,51	52,01	173,51	29,78	141,53	10,50	0,37	2,27	0,26	1,92	340,65
SUMW03A.US1.1	12,65	91,76	1027,27	47,54	989,66	27,79	84,13	11,81	4,03	40,73	61,94	9,37	50,80	8,56	0,11	1,28	1,00	1,82	136,10
SUM08B.US162.104	13,04	195,98	1217,04	41,54	1017,99	33,05	110,34	14,49	3,57	55,86	1039,72	19,54	75,96	12,60	0,19	1,92	2,39	3,99	95,14
IQM16B.US35.31	82,55	257,95	551,48	20,33	67,93	88,84	73,35	32,52	5,25	21,20	412,53	22,48	292,83	25,94	0,37	3,22	0,17	0,52	372,43
IQM16B.US30.6	77,71	286,81	483,30	24,50	70,10	85,87	78,22	35,43	5,41	21,36	330,61	26,07	249,72	22,27	0,33	2,97	0,14	0,56	123,31
IQM17A.US35.16	85,69	253,54	551,40	21,16	71,02	87,97	73,21	34,32	5,44	20,99	343,17	22,91	295,41	25,62	0,38	3,27	0,15	0,52	324,14
IQM16B.US30.3	75,28	260,64	426,45	26,83	74,14	92,33	79,53	35,60	5,67	18,15	265,04	25,57	240,34	22,27	0,32	2,84	0,13	0,54	129,18
IQM17A.US35.18	77,02	242,74	450,61	29,72	79,70	96,60	80,63	34,15	5,82	18,80	331,85	27,00	254,25	23,72	0,36	3,10	0,18	0,54	385,61
SUM11A.US174.232	26,12	255,32	1070,10	60,21	374,75	121,00	125,84	17,10	3,17	35,54	217,59	24,80	120,62	13,75	0,27	2,45	0,62	2,08	190,23
SUM09A.US297.2	18,01	258,65	128,04	37,71	85,15	129,47	88,79	24,29	2,92	11,64	193,36	21,17	60,24	10,97	0,13	2,28	0,23	0,72	117,18
SUM08B.US975.4	29,62	364,41	599,69	53,06	130,26	134,56	128,06	20,08	3,39	30,57	243,89	23,88	122,08	14,35	0,26	1,91	0,40	0,97	265,10
SUM11A.US54.85	22,12	243,04	140,47	30,31	72,19	93,08	80,66	21,45	3,10	75,15	249,49	24,98	98,43	15,71	0,16	2,56	0,56	4,28	277,90
SUM10A.US412.1	25,09	219,06	107,17	28,32	62,56	142,23	100,69	19,60	3,44	59,66	162,68	27,28	72,69	15,74	0,27	2,84	0,52	2,84	278,51
SUM10C.US174.104	26,66	200,99	113,65	35,47	71,60	122,25	98,38	20,94	4,16	65,85	260,38	27,29	120,68	16,16	0,41	3,31	0,34	2,32	305,56
SUM10C.US174.83	22,61	217,98	110,84	28,94	58,06	120,95	104,41	18,17	3,07	61,35	275,21	24,76	93,26	15,20	0,19	3,57	0,38	2,09	306,08
IQM16B.US30.10	19,15	134,80	149,88	21,51	97,04	53,47	99,01	18,71	2,85	99,88	445,95	20,59	80,14	13,21	0,25	2,81	0,50	6,83	278,26
SUM10C.US162.119	16,55	154,90	158,25	22,66	113,44	79,01	103,57	20,58	3,27	118,89	226,37	23,09	61,39	16,24	0,23	3,13	0,75	9,33	285,27
IQM18A.US80.3	19,47	153,40	165,09	24,05	115,10	49,90	86,20	20,36	3,12	111,90	302,23	22,07	86,62	14,35	0,35	3,02	0,49	8,47	426,96
SUM10A.US405.3	19,14	148,72	175,26	22,19	75,92	49,83	98,02	27,55	4,56	69,96	366,09	21,97	8,82	14,97	0,17	2,50	0,45	1,78	1452,53
IQM16B.US35.9	20,79	103,94	150,40	11,72	58,13	31,75	79,00	31,03	4,10	101,18	273,15	28,23	55,40	19,95	0,15	2,23	0,20	2,05	709,30

IQM17B.US73.1	19,42	88,60	196,54	12,21	75,13	25,59	74,31	33,85	4,51	68,55	113,88	21,71	86,77	39,76	0,16	4,00	0,42	4,06	429,89
IQM16B.US23.13	20,91	113,04	147,79	13,62	60,70	22,24	84,92	34,69	4,42	105,85	237,34	28,44	58,00	21,14	0,23	2,20	0,20	2,30	617,94
SUM08A.US253.5	21,16	125,37	172,21	11,94	61,21	40,80	66,04	28,65	4,69	82,57	456,31	21,81	46,39	14,37	0,13	2,26	0,24	1,57	1550,12
SUM10C.US174.79	22,01	163,49	157,65	14,70	80,37	42,48	87,30	34,66	4,61	37,77	238,95	21,96	54,25	20,01	0,14	3,20	0,27	1,47	1174,41
SUM03A.US133.9	18,01	136,18	143,13	11,02	48,46	32,58	106,88	33,60	5,72	86,80	69,35	20,32	41,89	45,28	0,12	2,44	0,48	2,17	432,15
SUM03B.US93.23	14,31	111,55	134,60	14,46	56,27	27,72	88,51	14,11	2,42	76,80	1474,40	20,16	64,46	10,28	0,57	2,20	0,49	6,29	169,13
SUM09B.US309.4	14,49	112,21	193,46	16,03	76,14	32,24	72,92	13,40	2,43	81,90	324,51	22,14	30,47	10,09	0,27	2,08	0,57	6,32	205,59
SUM03B.US93.42	12,84	111,97	121,36	13,54	73,63	33,66	80,55	15,46	2,63	102,91	3201,64	15,94	16,36	10,26	0,41	2,83	0,63	9,94	222,26

Table 7: Trace elements composition per sample (ppm). (cont.)

Sample Name	La	Ce	Pr	Nd	Sm	Eu	Gd	Tb	Dy	Ho	Er	Tm	Yb	Lu	Hf	Pb	Bi	Th	U
IQM16B.US35.8	14,73	34,80	4,02	14,58	3,75	0,65	2,60	0,39	2,22	0,43	1,09	0,17	0,95	0,15	1,25	9,40	0,15	5,10	1,38
IQM17A.US58.5	11,26	26,85	2,67	10,67	2,42	0,52	1,86	0,28	1,64	0,31	0,78	0,12	0,83	0,11	1,01	12,61	0,10	4,14	1,02
IQM18B.US119.5	12,59	26,75	3,20	7,84	2,99	0,71	2,09	0,31	2,02	0,40	0,93	0,16	0,99	0,13	1,27	7,66	0,02	3,43	2,22
IQM17A.US58.8	16,85	37,07	4,60	16,77	4,40	0,92	3,31	0,54	3,42	0,69	1,74	0,29	1,68	0,25	2,49	9,68	0,05	4,20	1,44
IQM16B.US35.34	22,96	51,71	6,39	23,28	6,06	1,23	4,11	0,63	3,77	0,73	1,72	0,29	1,60	0,24	2,53	11,47	0,03	4,78	1,66
IQM16B.US35.35	21,72	48,39	6,00	21,67	6,09	1,09	4,39	0,73	4,80	0,98	2,33	0,40	2,25	0,33	3,46	16,08	0,02	5,14	1,60
IQM16B.US35.33	22,15	50,22	6,22	25,52	5,23	1,18	4,48	0,69	4,33	0,86	2,25	0,36	2,48	0,36	3,55	11,78	0,14	4,93	1,73
IQM16B.US35.32	25,00	56,66	7,22	30,35	6,06	1,38	5,34	0,82	5,25	1,04	2,56	0,42	2,83	0,38	3,57	8,01	0,15	5,22	1,27
SUMW03A.US1.1	11,22	28,15	2,33	8,86	1,93	0,45	1,60	0,27	1,73	0,34	0,86	0,14	0,97	0,13	1,43	11,27	0,04	4,65	1,46
SUM08B.US162.104	22,36	49,14	5,42	18,57	3,86	0,78	3,52	0,54	3,53	0,72	1,87	0,31	1,87	0,30	2,47	26,78	0,09	7,12	2,44
IQM16B.US35.31	18,04	45,78	6,30	25,44	9,04	2,38	5,43	0,96	6,36	1,16	2,59	0,45	2,60	0,35	7,45	6,81	0,04	7,98	1,60
IQM16B.US30.6	18,59	54,79	7,50	30,15	10,57	2,36	6,84	1,27	8,02	1,47	3,44	0,55	3,04	0,44	6,69	6,36	0,06	7,04	1,55
IQM17A.US35.16	18,75	46,52	6,56	24,51	9,32	2,32	5,58	1,00	6,60	1,21	2,70	0,47	2,58	0,36	7,52	6,22	0,06	7,76	1,64
IQM16B.US30.3	17,11	40,51	7,18	32,88	9,23	2,55	6,89	1,18	7,44	1,34	3,14	0,49	3,33	0,44	5,80	7,44	0,09	6,27	1,45
IQM17A.US35.18	20,00	53,94	8,07	36,31	9,73	2,87	7,56	1,27	8,01	1,43	3,33	0,52	3,53	0,45	6,26	8,71	0,07	6,86	1,45
SUM11A.US174.232	23,05	52,51	6,30	25,66	6,10	1,47	5,46	0,84	5,10	0,99	2,53	0,37	2,09	0,33	3,48	160,59	0,08	6,96	1,21
SUM09A.US297.2	11,61	29,56	3,78	16,75	4,59	1,38	4,19	0,69	4,36	0,87	2,26	0,33	1,87	0,29	1,80	11,29	0,03	1,74	0,58
SUM08B.US975.4	16,59	42,12	4,93	18,89	5,27	1,42	4,68	0,78	5,01	0,96	2,53	0,36	2,07	0,32	4,08	19,00	0,01	3,57	0,85
SUM11A.US54.85	26,25	57,95	6,67	24,55	5,40	1,34	5,19	0,78	4,92	0,96	2,28	0,37	2,12	0,33	2,77	22,93	0,01	8,50	1,44
SUM10A.US412.1	26,56	54,39	6,73	26,37	6,24	1,41	5,32	0,86	5,25	1,03	2,76	0,39	2,20	0,34	3,16	69,71	0,05	9,42	1,42
SUM10C.US174.104	28,80	61,86	7,21	24,53	5,54	1,48	5,18	0,78	4,91	0,93	2,18	0,35	2,25	0,28	2,89	38,31	0,14	8,58	1,28
SUM10C.US174.83	24,32	51,92	6,16	23,31	5,19	1,31	4,93	0,76	4,77	0,93	2,24	0,35	2,04	0,32	2,61	40,89	0,08	7,78	1,25
IQM16B.US30.10	25,58	55,32	6,29	20,26	5,59	1,30	4,10	0,63	3,94	0,78	1,86	0,31	1,77	0,25	2,32	16,35	0,11	9,58	1,63
SUM10C.US162.119	29,86	64,47	7,40	24,42	5,39	1,15	4,87	0,71	4,33	0,85	2,16	0,34	1,98	0,31	2,23	70,81	0,25	11,92	1,79
IQM18A.US80.3	30,71	64,24	7,43	28,24	5,32	1,23	4,69	0,68	4,04	0,79	1,97	0,31	2,13	0,29	2,24	24,05	0,05	12,69	1,78
SUM10A.US405.3	63,08	128,33	13,54	47,56	8,77	2,05	6,78	0,87	4,72	0,87	2,29	0,31	1,81	0,28	1,53	242,39	0,03	13,91	0,96

IQM16B.US35.9	47,14	107,73	11,14	39,09	9,61	1,94	6,67	0,99	6,16	1,18	2,69	0,46	2,56	0,36	1,69	36,30	0,16	14,94	2,69
IQM17B.US73.1	65,11	135,25	14,12	49,72	10,57	1,64	6,71	0,88	5,04	0,92	2,12	0,35	2,05	0,27	2,54	38,41	0,20	25,42	4,52
IQM16B.US23.13	56,72	124,69	13,20	49,75	9,14	1,91	7,53	1,03	6,03	1,14	2,77	0,43	2,91	0,40	1,59	48,41	0,28	19,18	2,77
SUM08A.US253.5	63,45	128,39	13,54	50,10	7,72	2,50	6,50	0,79	4,25	0,77	1,85	0,27	1,77	0,22	1,43	58,11	0,09	13,43	1,62
SUM10C.US174.79	52,53	115,10	12,09	42,81	6,89	2,19	6,32	0,82	4,71	0,86	2,04	0,31	2,01	0,24	1,72	87,40	0,09	14,51	1,27
SUM03A.US133.9	85,42	193,67	21,42	78,09	12,63	1,32	9,90	1,10	5,27	0,91	2,15	0,33	2,01	0,31	2,01	42,88	0,17	46,13	4,95
SUM03B.US93.23	24,74	50,41	6,13	22,73	5,17	0,98	4,31	0,63	3,81	0,75	2,08	0,29	1,73	0,27	2,14	15,11	0,15	10,50	1,68
SUM09B.US309.4	24,21	49,88	5,78	19,20	4,65	0,94	4,14	0,62	3,85	0,77	2,06	0,30	1,76	0,28	1,61	29,11	0,10	9,26	1,43
SUM03B.US93.42	21,82	45,99	5,42	20,46	4,14	0,77	3,40	0,55	3,13	0,60	1,65	0,25	1,47	0,23	1,80	17,29	0,13	10,52	1,90

Table 8: BSE images of the different groups with elemental mapping.

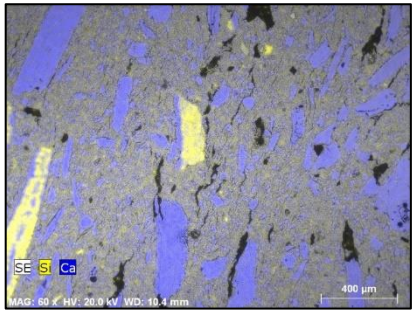

BSE image of **ST** group with the distribution of Si (yellow) and Ca (blue) both composing shell fragments.

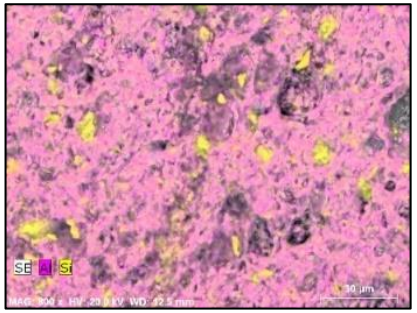

BSE image of shale grain in **SF** group with the distribution of Al (pink-paste) and Si (yellow-quartz grains).

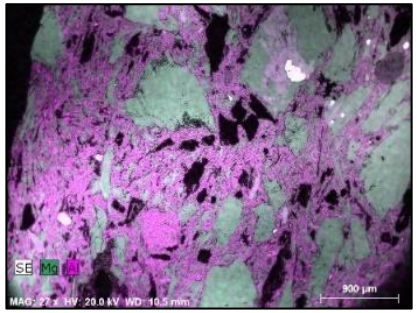

BSE image of **TF** group with the distribution of Mg (green-talc) and Al (pink-paste).

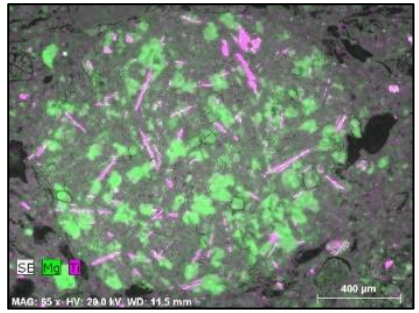

BSE image of basalt grain in **BF** with the distribution of Mg (green-pyroxene) and Ti (pink-oxide).

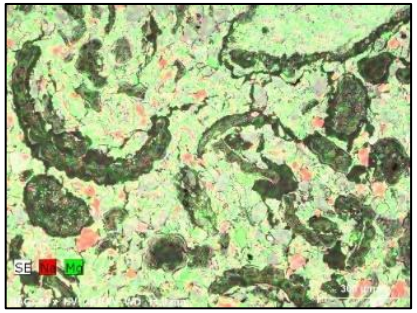

BSE image of **RT** group with the rice husk imprints and the distribution of Mg (green-paste) and Na (red-plagioclase).

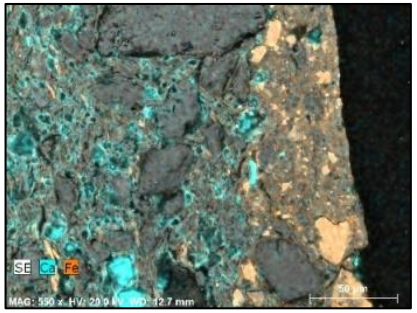

BSE image of **FF** group with the distribution of Ca (blue-pores, bone fragments and plagioclase) concentrated in the inner body and Fe (orange-micas) concentrated on the surface.

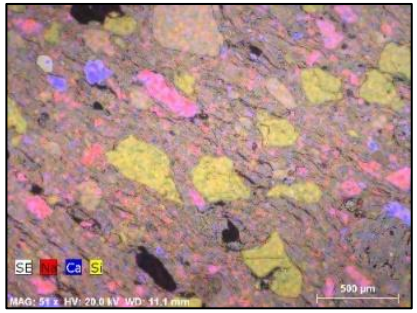

BSE image of **MLF** group with the distribution of Na (red- feldspar), Ca (blue-amphiboles) and Si (yellow-quartz).

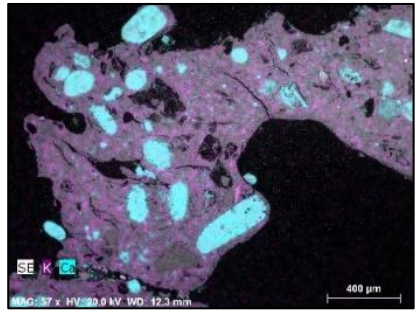

BSE image of **SFF** group with the distribution of K (purple-paste) and Ca (blue-calcitic shell).

Figures:

Figure 1: Mute map of Oman with the location of the Khor Rori archaeological site being highlighted

Figure 2: Major Element (wt.%) comparison of one representative sample per group. ST: Shell Tempered; SF: Shale-rich Fabric; TF: Talc-rich Fabric; BF: Basalt-rich Fabric; RT: Rice Tempered; FF: Fine Fabric; MLF: Medium-Large inclusions in fine Fabric; SSF: Shell and Sand rich Fabric

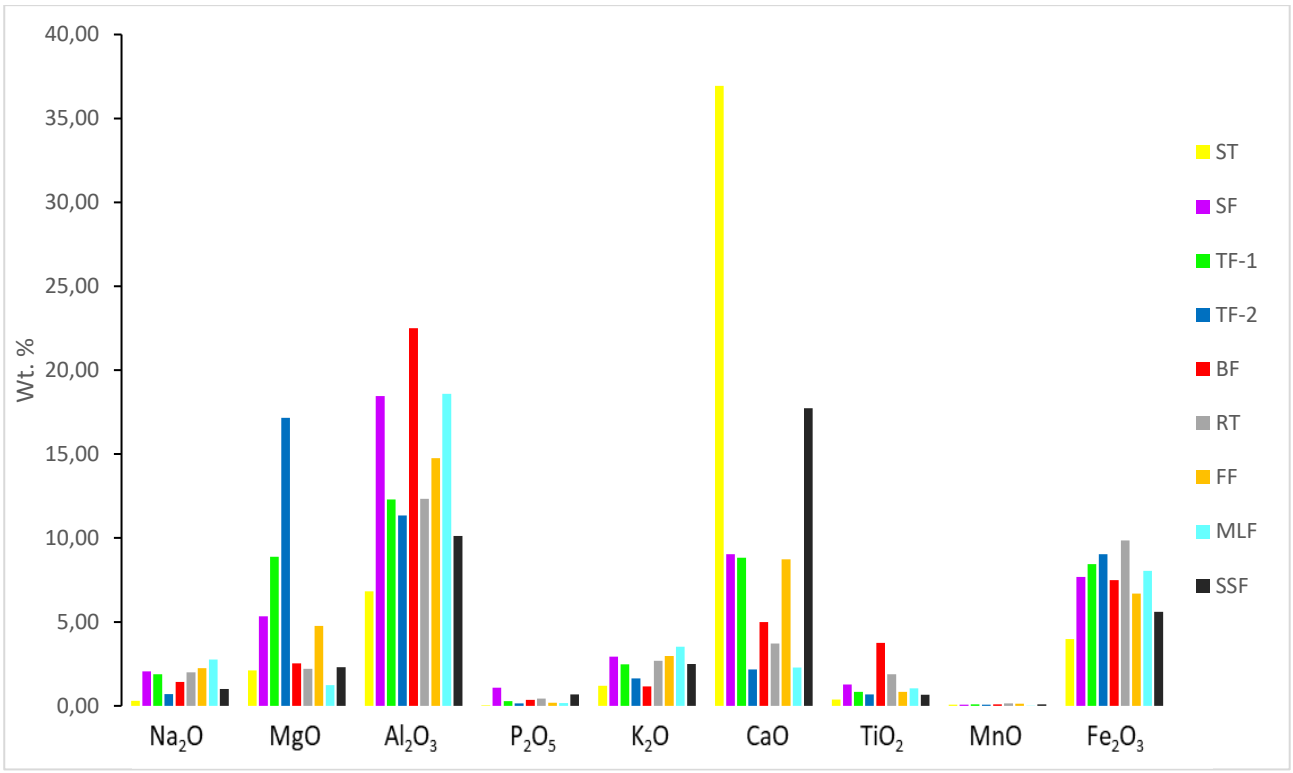

Figure 3: major oxide composition plots of the different groups. The images should be combined into one single one with groups being from left to right and top to bottom in the following order: ST (yellow), SF (purple),TF (green and blue), BF (red),RT (grey), FF (green), MLF (blue), SSF (brown).

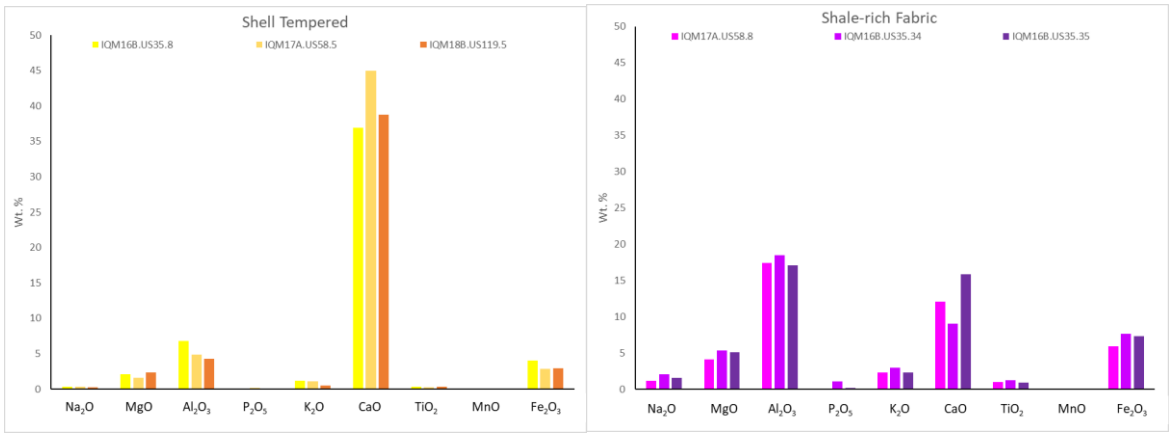

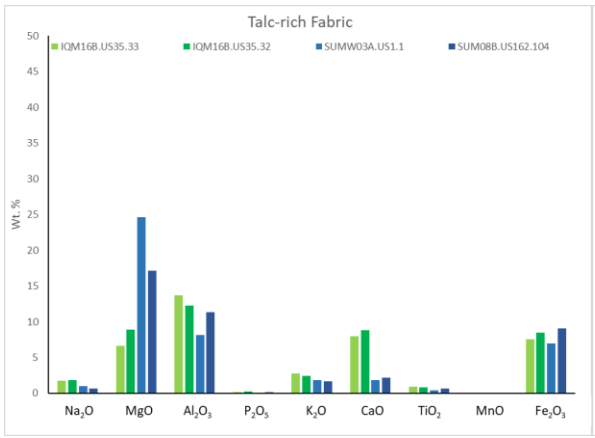
Talc-rich Fabric
IQM16B.US35.33
IQM16B.US35.32
SUMW03A.US1.1
SUM08B.US162.104
Wt. %
Na2O MgO Al2O3 P2O5 K2O CaO TiO2 MnO Fe2O3

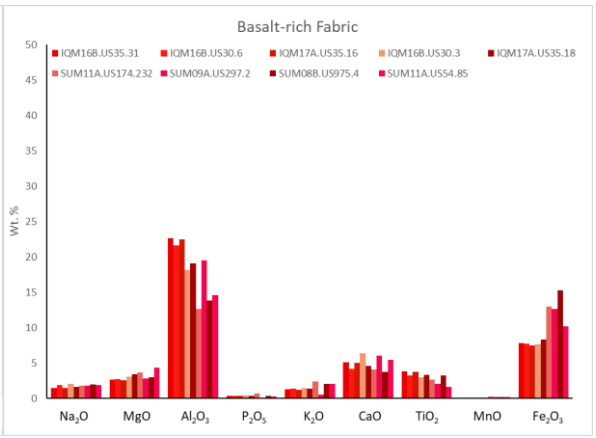
Basalt-rich Fabric
IQM16B.US35.31
IQM16B.US30.6
IQM17A.US35.16
IQM16B.US30.3
IQM17A.US35.18
SUM11A.US174.232
SUM09A.US297.2
SUM08B.US975.4
SUM11A.US54.85
Wt. %
Na2O MgO Al2O3 P2O5 K2O CaO TiO2 MnO Fe2O3

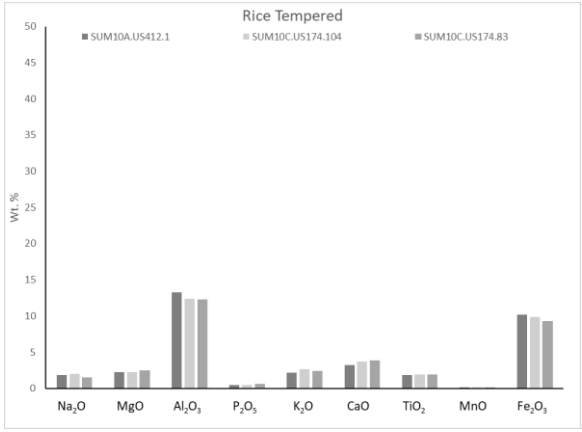
Rice Tempered
SUM10A.US412.1
SUM10C.US174.104
SUM10C.US174.83
Wt. %
Na2O MgO Al2O3 P2O5 K2O CaO TiO2 MnO Fe2O3

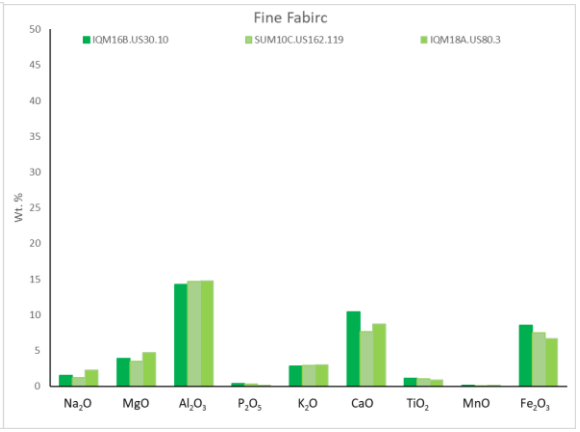
Fine Fabirc
IQM16B.US30.10
SUM10C.US162.119
IQM18A.US80.3
Wt. %
Na2O MgO Al2O3 P2O5 K2O CaO TiO2 MnO Fe2O3

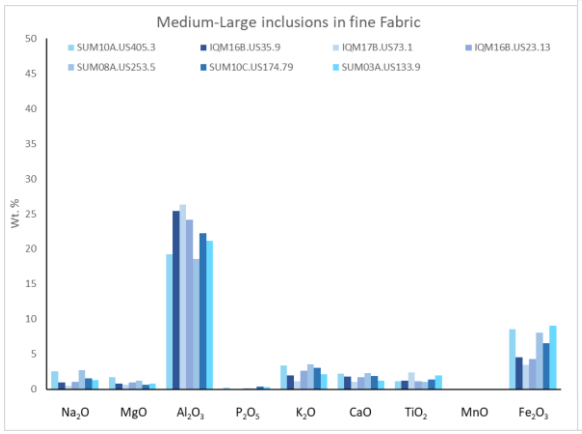
Medium-Large inclusions in fine Fabric
SUM10A.US405.3
IQM16B.US35.9
IQM17B.US73.1
IQM16B.US23.13
SUM08A.US253.5
SUM10C.US174.79
SUM03A.US133.9
Wt. %
Na2O MgO Al2O3 P2O5 K2O CaO TiO2 MnO Fe2O3

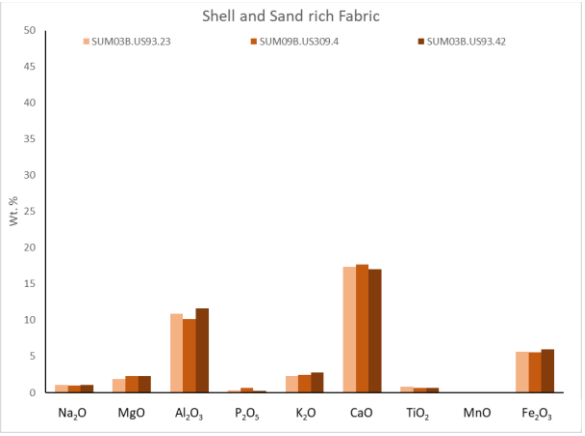
Shell and Sand rich Fabric
SUM03B.US93.23
SUM09B.US309.4
SUM03B.US93.42
Wt. %
Na2O MgO Al2O3 P2O5 K2O CaO TiO2 MnO Fe2O3

Figure 4: Ternary diagram (after Heimann and Maggetti 2019) of major oxides in correspondence of Al_2O_3, SiO_2 and CaO+MgO with local in the blue circle and Indian in red circle stylistically identified. ST: Shell Tempered; SF: Shale-rich Fabric; TF: Talc-rich Fabric; BF: Basalt-rich Fabric; RT: Rice Tempered; FF: Fine Fabric; MLF: Medium-Large inclusions in fine Fabric; SSF: Shell and Sand rich Fabric.

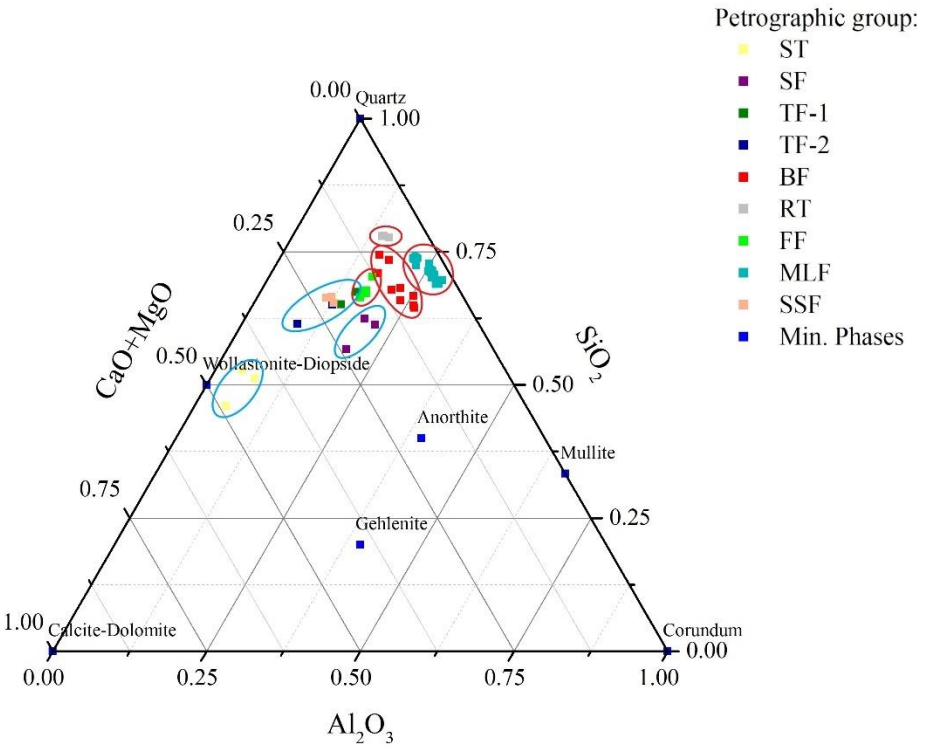

Figure 5: Ternary diagram of pyroxenes from BF samples and RT samples. The comparison is also among pyroxene located within basalt grains (crossed empty symbol) and single pyroxene grains (full coloured symbols), both within BF samples (after Heimann and Maggetti 2019).

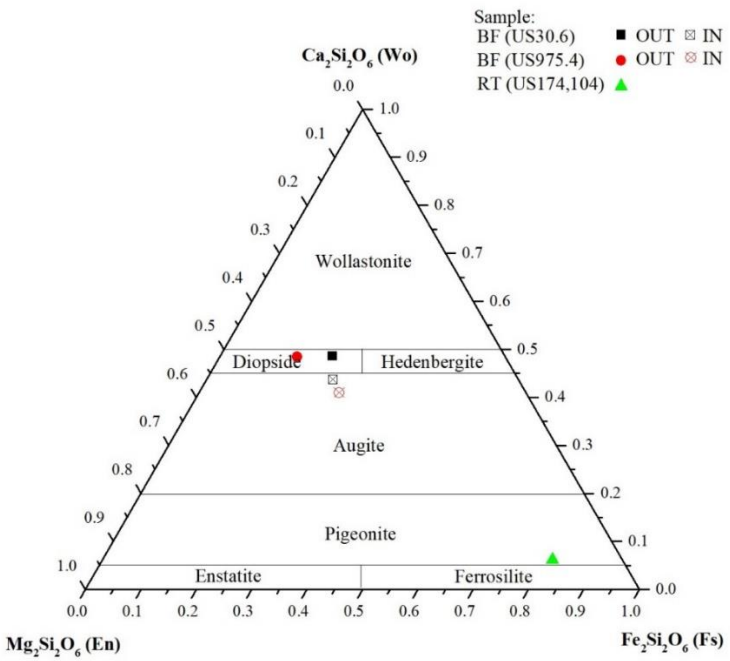

Figure 6: Ternary plot (after Heimann and Maggetti 2019) representing the comparison of the binders according to CaO + MgO, SiO_2 and Al_2O_3 (wt.%). ST: Shell Tempered; SF: Shale-rich Fabric; TF: Talc-rich Fabric; BF: Basalt-rich Fabric; RT: Rice Tempered; FF: Fine Fabric; MLF: Medium-Large inclusions in fine Fabric; SSF: Shell and Sand rich Fabric.

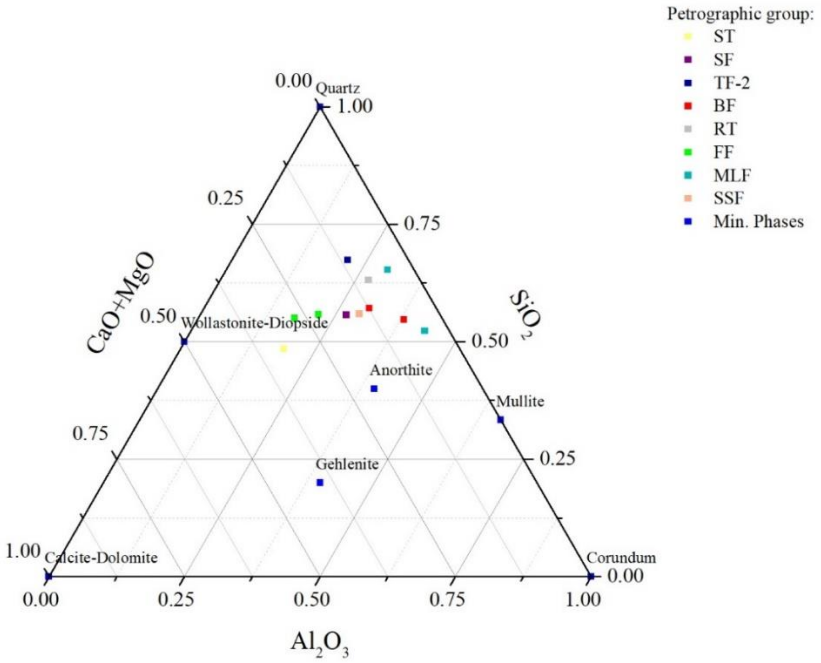

Figure 7: Binary plot comparing Al_2O_3/SiO_2 and MgO/SiO_2 with Arabic samples identified within the dots on the plot and Indian samples within triangles. ST: Shell Tempered; SF: Shale-rich Fabric; TF: Talc-rich Fabric (TF-2 samples are not ploted for better visualisation with TF-2 MgO/SiO_2 ratio being above 0.30); BF: Basalt-rich Fabric; RT: Rice Tempered; FF: Fine Fabric; MLF: Medium-Large inclusions in fine Fabric; SSF: Shell and Sand rich Fabric.

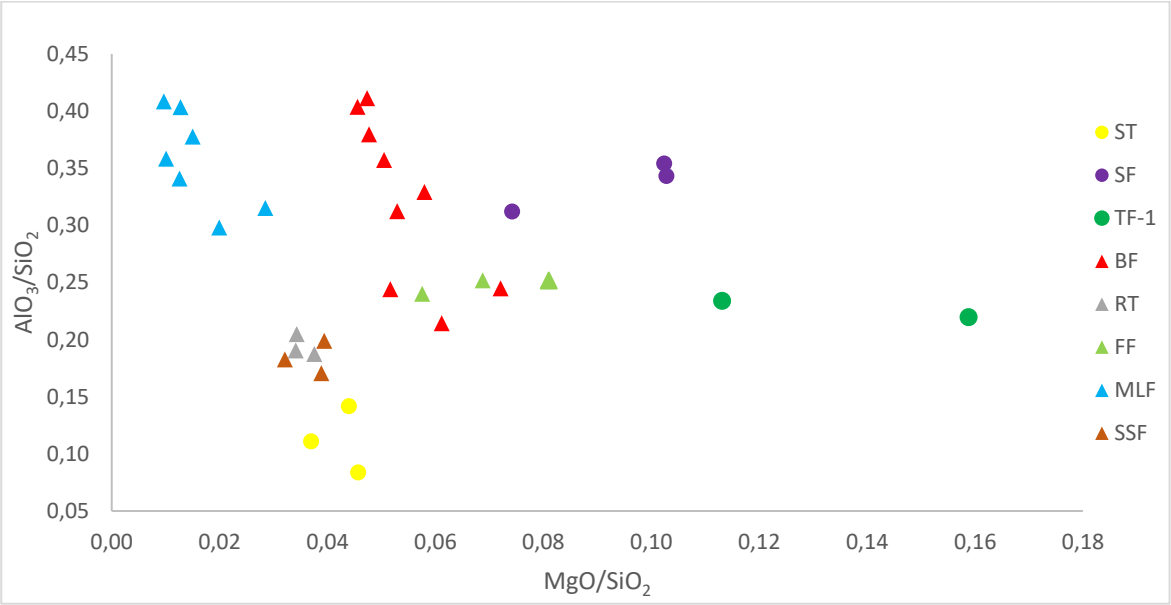

Figure 8: Comparison between TF samples (blue and green) and stoneware samples from UAE in yellow (Magee et al. 2005).

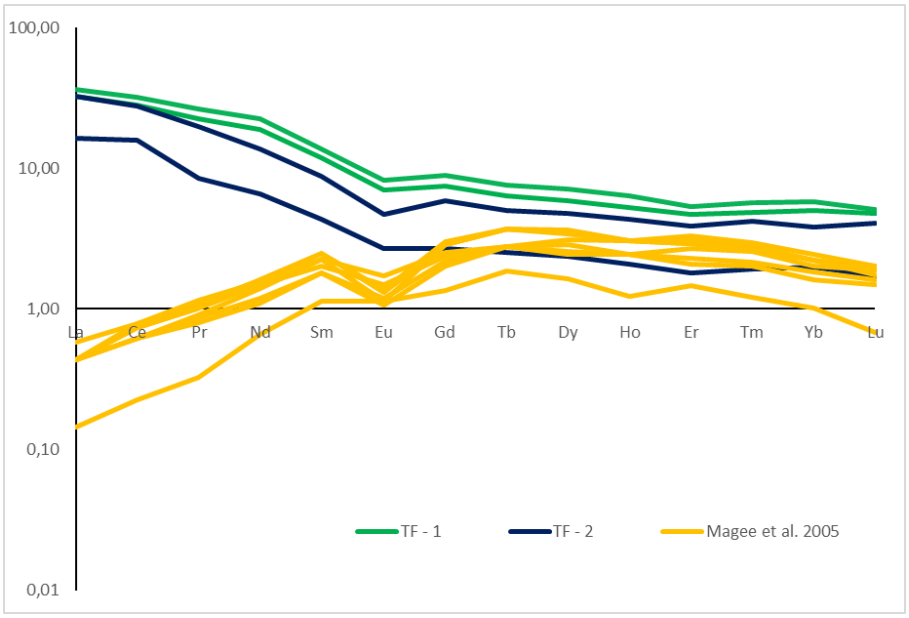

Figure 9: Graphic comparison of the samples from MLF (blue) with sample trace element composition from Arikamedu, Chandraketugarh and Tamluk (yellow) (Das et al. 2017)

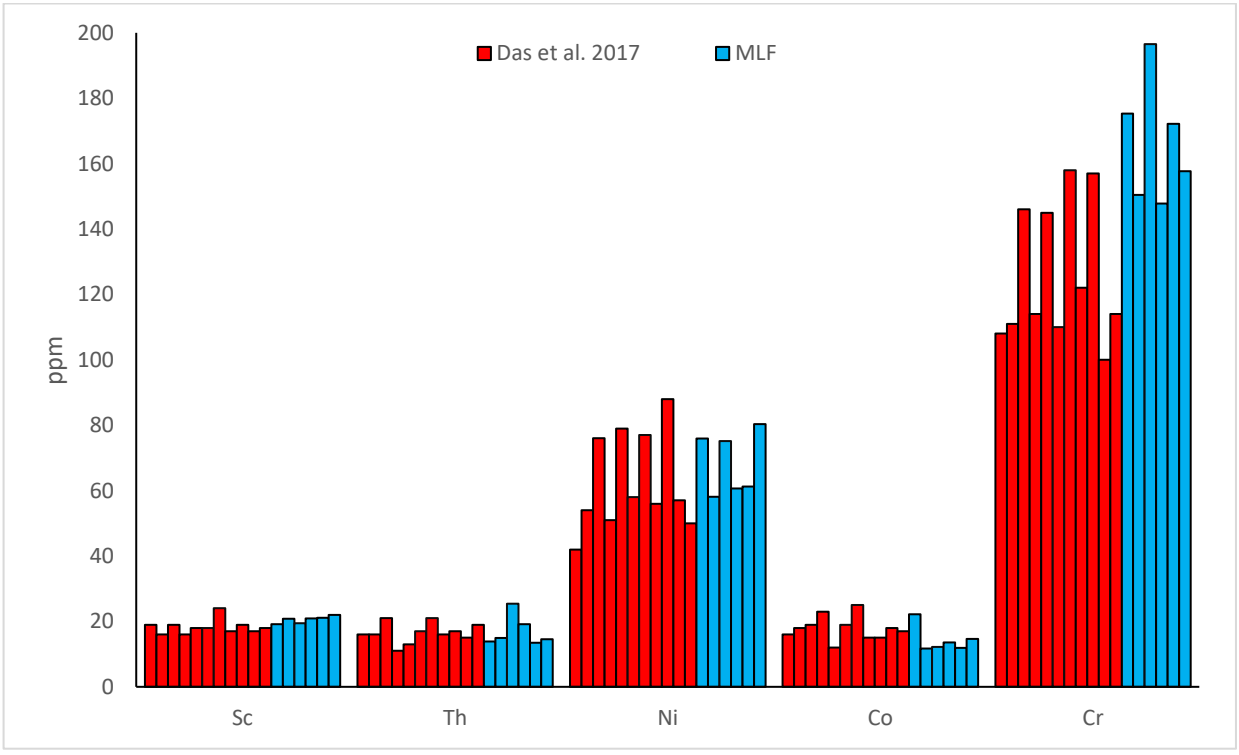

Figure 10 Graphic comparison of the samples from MLF (blue) with sample oxide composition from Vellore (yellow) (Naseerutheen et al. 2014);

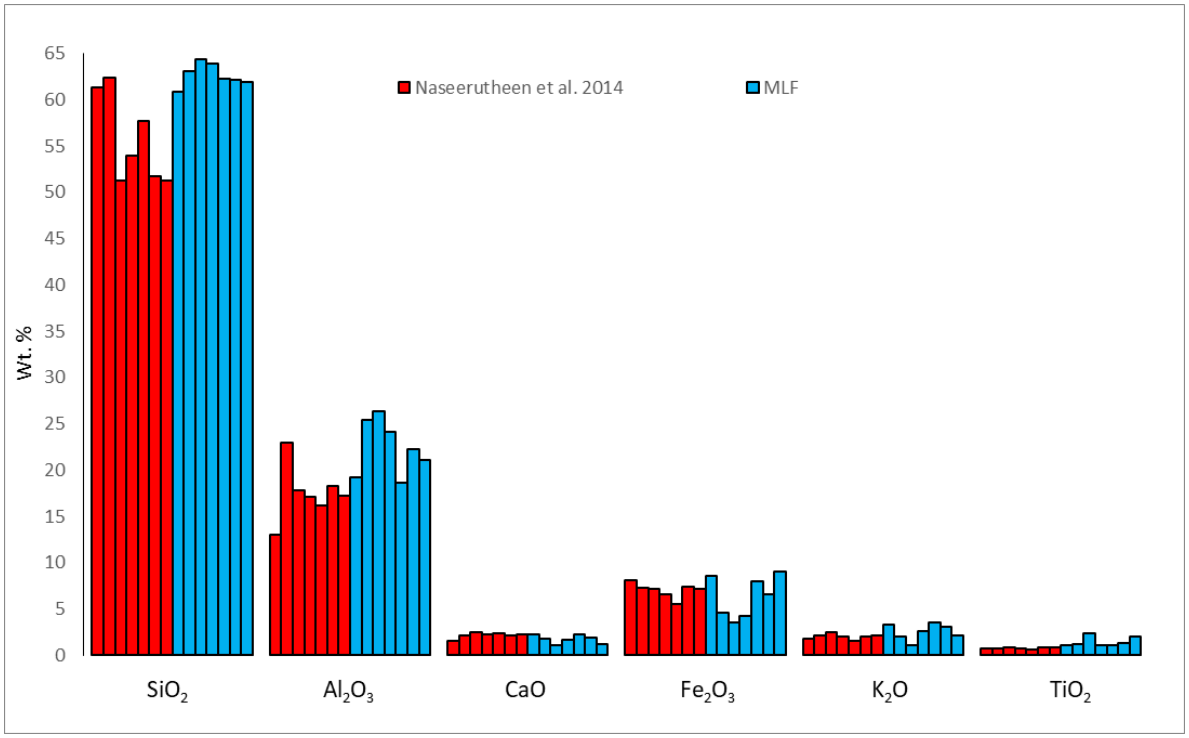

Figure 11: Map of the identified area of provenance.